JCI The Journal of Clinical Investigation

FoxO3 activation in hypoxic tubules prevents chronic kidney disease

Ling Li, … , Qais Al-Awqati, Fangming Lin

J Clin Invest. 2019;129(6):2374-2389. https://doi.org/10.1172/JCI122256.

Research Article | Cell biology | Nephrology

Graphical abstract

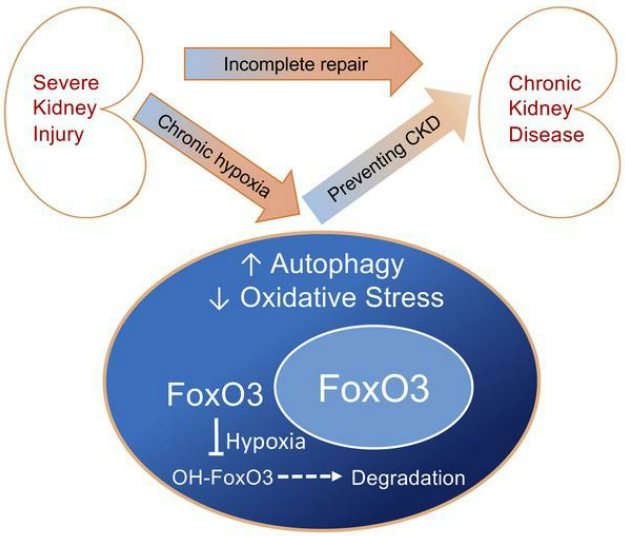

FoxO3 activation in hypoxic tubules prevents chronic kidney disease

Ling Li,[1] Huimin Kang,[1,2] Qing Zhang,[3] Vivette D. D'Agati,[4] Qais Al-Awqati,[5] and Fangming Lin[1]

[1]Department of Pediatrics, Columbia University Vagelos College of Physicians and Surgeons, New York, New York, USA. [2]Department of Pediatrics, Fujian Medical University Union Hospital, Fuzhou, Fujian, China. [3]Department of Pathology and Laboratory Medicine, University of North Carolina, Chapel Hill, North Carolina, USA. [4]Department of Pathology and [5]Department of Internal Medicine, Columbia University Vagelos College of Physicians and Surgeons, New York, New York, USA.

Acute kidney injury (AKI) can lead to chronic kidney disease (CKD) if injury is severe and/or repair is incomplete. However, the pathogenesis of CKD following renal ischemic injury is not fully understood. Capillary rarefaction and tubular hypoxia are common findings during the AKI-to-CKD transition. We investigated the tubular stress response to hypoxia and demonstrated that a stress-responsive transcription factor, FoxO3, was regulated by prolyl hydroxylase (PHD). Hypoxia inhibited FoxO3 prolyl hydroxylation and FoxO3 degradation, leading to FoxO3 accumulation and activation in tubular cells. Hypoxia-activated HIF-1α contributed to FoxO3 activation and functioned to protect kidneys, as tubular deletion of HIF-1α decreased hypoxia-induced FoxO3 activation and resulted in more severe tubular injury and interstitial fibrosis following ischemic injury. Strikingly, tubular deletion of FoxO3 during the AKI-to-CKD transition aggravated renal structural and functional damage, leading to a much more profound CKD phenotype. We show that tubular deletion of FoxO3 resulted in decreased autophagic response and increased oxidative injury, which may explain renal protection by FoxO3. Our study indicates that in the hypoxic kidney, stress-responsive transcription factors can be activated for adaptions to counteract hypoxic insults, thus attenuating CKD development.

Introduction

When acute renal failure was recognized as a syndrome more than 70 years ago, it was considered to be an acute injury to the kidney, which more often than not resulted in recovery of renal function. A separate syndrome of chronic renal failure became known, and the two were thought to differ in etiology and natural history. Recent epidemiological and case-controlled studies using new definitions of the 2 syndromes indicate that acute kidney injury (AKI) and chronic kidney disease (CKD) are interconnected (1). AKI increases the risk for CKD by 8.8-fold and the risk for end-stage renal disease (ESRD) requiring dialysis or kidney transplantation by 3.3-fold (2).

The pathogenesis of AKI leading to CKD has been under intensive study, with many investigators using animal models of ischemia-reperfusion injury (IRI). Mild ischemic injury triggers intrinsic repair mechanisms that result in replacement of damaged cells and complete functional recovery (3, 4). With more severe injury, the repair processes fail to completely ameliorate the damage, and animals develop CKD (5, 6). The severity of ischemic injury induced by clamping of renal blood vessels can be readily modified by changing the duration of warm ischemia. A severe injury induced by 45 minutes of ischemia results in profound tubular damage, with loss of brush border in proximal tubules, diffused cell detachment from the basement membrane, extensive cast formation in tubular lumens, and intense interstitial inflammation. Repair of tubular epithelia following severe injury is largely mediated by dedifferentiation, proliferation, migration, and redifferentiation of surviving tubular cells. Most published animal studies of IRI have investigated renal repair for short periods of time following the acute ischemic phase. Long-term follow-up studies have shown that, following severe IRI, the kidneys develop tubular atrophy (7) resulting in impaired nephron architecture and function. Tubular atrophy and fibrosis are the hallmarks of CKD. Sequential examinations for weeks in a model of severe IRI have allowed us to investigate the pathogenesis of AKI-to-CKD transition at cellular and molecular levels. We aimed to understand the cellular defense mechanism that promotes survival and repair. Given that ischemia is a strong stress signal, autophagy could be a mechanism, since it is an evolutionarily conserved stress response. Autophagy recycles intracellular constituents and removes damaged organelles to maintain cellular homeostasis. In kidneys with severe injury and incomplete repair, chronic hypoxia develops, probably as a result of peritubular capillary rarefaction (8, 9). Hypoxia and metabolic perturbation are 2 of the major inducers of autophagy (10). We reasoned that autophagy in response to hypoxia could be at the root of renal injury and repair. With chronic hypoxia, autophagy as a compensatory mechanism may not be sufficient to allow renal structure and function to return to the pristine stage.

Here, we studied the relationship between hypoxia and autophagy and found that hypoxia activates a stress-responsive tran-

▶ Related Commentary: p. 2192

Conflict of interest: The authors have declared that no conflict of interest exists.

Submitted: May 22, 2018; **Accepted:** March 19, 2019; **Published:** May 6, 2019.
Reference information: *J Clin Invest*. 2019;129(6):2374–2389.
https://doi.org/10.1172/JCI122256.

scription factor, FoxO3, a major regulator of epithelial autophagy in the kidney, as we recently demonstrated (11). We provide evidence to show that, like HIF-1α transcription factors, FoxO3 can be hydroxylated at proline residues in the presence of molecular oxygen. During renal hypoxia, prolyl hydroxylation and FoxO3 degradation are inhibited, thereby increasing FoxO3 protein abundance and leading to its activation and stimulation of stress responses including epithelial autophagy. Furthermore, tubular deletion of FoxO3 during the AKI-to-CKD transition reduces autophagy and aggravates oxidative damage, leading to profound pathological changes resembling the CKD phenotype. We believe our results demonstrate a previously unrecognized function of the pleotropic transcription factor FoxO3 in regulating renal stress responses and ameliorating the severity of CKD.

Results

FoxO3 transcription factor is activated in hypoxic renal tubules. To understand the pathogenesis of the AKI-to-CKD transition, we examined acute and long-term responses of mouse kidneys following severe injury induced by 45 minutes of IRI. Whereas acute injury triggers cell proliferation and tubular repair (Supplemental Figure 1; supplemental material available online with this article; https://doi.org/10.1172/JCI122256DS1), renal repair is often incomplete. Specifically, we found evidence of partial recovery at 1 week. At 2 weeks, focal atrophic tubules began to appear as kidneys transitioned to CKD. At 4 weeks, CKD developed with areas of tubular atrophy, interstitial fibrosis, and chronic inflammation (Figure 1A). The density of renal microvessels identified by the endothelial marker endomucin was found to be markedly reduced. This reduction in microvessels was associated with tubular hypoxia, shown by an increased intensity of the hypoxia-dependent pimonidazole protein adducts (Figure 1B). Since hypoxia is a potent inducer of autophagy, we examined the conversion of LC3I to LC3II, a commonly used biochemical assay for autophagy, during the period of CKD development. We found that the ratio of LC3II/LC3I was significantly increased (Figure 1C). We also demonstrated that there was an increase in autophagy using autophagy reporter *CAG-RFP-EGFP-LC3* (*CREL*) mice (12), by showing increased fluorescent dots in tubules surrounding areas of low capillary density (Figure 1D).

Next, we investigated hypoxia-induced autophagy through the activation of the stress-responsive transcription factor FoxO3, which has been shown to regulate renal epithelial autophagy in kidneys with obstructive injury (11). We found that FoxO3 was activated in renal tubules during the AKI-to-CKD transition (Figure 1E). By 4 weeks after IRI, 29.1% ± 2.9% of tubular cells expressed nuclear FoxO3 from a baseline of 5.9% ± 1.2% in uninjured kidneys, suggesting activation of the FoxO3 transcription factor during chronic hypoxia.

Hypoxia increases FoxO3 protein abundance by inhibiting its prolyl hydroxylation. To exert its effect, FoxO3 needs be located in the nucleus, where it acts as a transcription factor. To understand the role of hypoxia in FoxO3 activation, we used primary cultures of renal tubular cells grown in a medium known to promote proximal tubular cell growth (13). Cells were infected with adeno-FoxO3-GFP or control adeno-GFP viruses. Using a viral titer that produced low infection efficiency, an average of 17.7% cells expressed cytoplasmic GFP under normal culture conditions 24 hours after infection. Exposing cells to 1% O_2 resulted in nuclear accumulation of FoxO3-GFP that peaked at 30 minutes, at which point 65.6% ± 4% of infected cells showed a strong nuclear signal (Figure 2, A and B). Immunostaining of endogenous FoxO3 (without FoxO3 overexpression) indicated abundant nuclear FoxO3 in cells exposed to 1% O_2 (Figure 2C). Endogenous FoxO3 protein levels showed significant increases in response to hypoxia for 30 minutes to 2 hours (Figure 2D), while *FoxO3* mRNA levels did not change at the 60-minute time point (Supplemental Figure 2). These results suggest that hypoxia may regulate FoxO3 at the posttranslational level. One of the best-studied posttranslational regulations of FoxO3 is phosphorylation by AKT at Ser253, which is the crucial step causing phosphorylated FoxO3 (p-FoxO3) nuclear export to the cytoplasm, where it is degraded (14–17). We found that the accumulation of nuclear FoxO3 protein was accompanied by increased p-FoxO3 at Ser253. However, we did not detect a significant effect of hypoxia on AKT or p-AKT levels (Figure 2E), suggesting that nuclear FoxO3 accumulation under hypoxic conditions is probably not due to reduced FoxO3 nuclear export and that the increased p-FoxO3 may not be due to the change in AKT activity. Furthermore, while proximal tubules of the kidney had undetectable levels of p-FoxO3 at baseline or 4 weeks after IRI, nuclear FoxO3 increased from 6.0% ± 3.15% at baseline to 28.28% ± 15.6% 4 weeks after IRI (Figure 2F), supporting the conclusion that mechanisms other than AKT signaling are playing a role in the posttranslational regulation of FoxO3 protein abundance.

Although the hypoxia-induced increase in FoxO3 protein levels could be HIF dependent, recent studies suggest that FoxO3 can be directly affected by hypoxia. FoxO3 was found to be hydroxylated at Pro426 and Pro437 by prolyl hydroxylase 1 (PHD1), which depends on oxygen, α-ketoglutarate, iron, and ascorbic acid for its activity, similar to the regulation of α subunit of HIF proteins. Hydroxylation of FoxO3 prevents its binding to the USP9x deubiquitinase and promotes its proteasomal degradation (18). To examine whether hypoxia directly affects FoxO3 in kidney epithelia, we immunoprecipitated proteins isolated from renal epithelial cell cultures using the FoxO3 antibody followed by blotting with a pan-hydroxyl proline antibody. We found that there was reduced prolyl hydroxylated FoxO3 in cells grown in hypoxic conditions (1% O_2). Remarkably, treating cells grown in normal growth factor– and nutrient-rich conditions with the hypoxia mimetic dimethyloxalylglycine (DMOG), which inhibited PHD enzymes, also caused a 60% reduction in hydroxylated FoxO3 and a 39% increase in FoxO3 protein levels (Figure 2G). Similarly, depriving cells of amino acids and glucose increased the abundance of FoxO3 protein. Conversely, supplementing starved cells with a cell-permeable analog of α-ketoglutarate, dimethyl α-ketoglutarate (DMKG), resulted in a 57% decrease in FoxO3 protein (Figure 2H). PHD1, -2, and -3 enzymes, which are known to be expressed in renal tubular cells (19), showed no change in protein levels in cells exposed to hypoxia (Supplemental Figure 3). Taken together, our results indicate that FoxO3 protein can be regulated by the O_2- and α-ketoglutarate–dependent PHD enzymes in kidney epithelial cells. Hypoxia or a deficiency in α-ketoglutarate, a

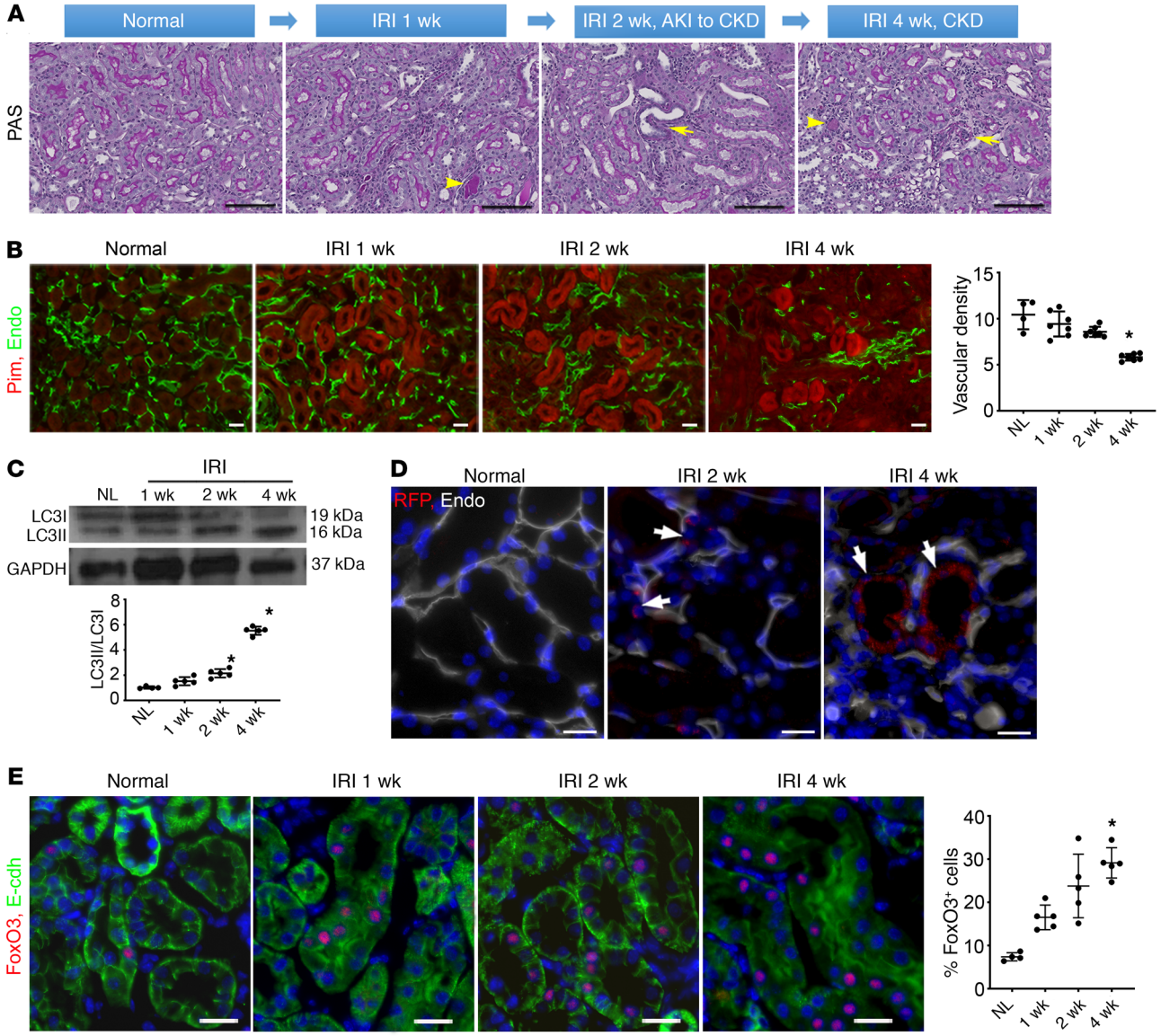

Figure 1. Severe renal IRI leads to CKD, hypoxia, and activation of autophagy and FoxO3. (**A**) Mice were subjected to 45 minutes of unilateral left renal IRI, and the kidneys were examined up to 4 weeks after IRI. Representative PAS stainings indicate partial repair and CKD development after initial IRI. Arrows denote tubular atrophy, and arrowheads indicate cast formation in the lumens of tubules. (**B**) Reduction of the density of renal microvessels is identified by the endothelial marker endomucin (Endo, green) and renal hypoxia is indicated by the intensity of the hypoxia-dependent pimonidazole protein adducts (Pim, red). $n = 4$ for normal controls; $n = 7$ for 1, 2, and 4 weeks after IRI. (**C**) Increased renal autophagy with a higher LC3II/LC3I ratio during CKD development. $n = 5$. GAPDH served as a loading control. (**D**) Appearance of autophagic dots (RFP dots, arrows) in tubules surrounding a low density of capillaries labeled with endomucin (Endo, white). (**E**) FoxO3 activation with nuclear expression (red) in renal tubules labeled with E-cadherin (green, E-cdh). $n = 4$ for normal controls; $n = 5$ for IRI at 1, 2, and 4 weeks. Nuclei were counterstained with DAPI (blue) in **D** and **E**. Scale bars: 100 μm (**A**), 50 μm (**B**), and 20 μm (**D** and **E**). *$P < 0.05$ compared with normal controls, by 1-way ANOVA followed by Dunnett's post hoc test for multiple comparisons (**B**, **C**, and **E**).

metabolic intermediate generated by the TCA cycle, prevents FoxO3 hydroxylation and reduces its degradation.

Next, we used a newly generated antibody to detect OH-FoxO3 at Pro437 (MilliporeSigma, ABE1848). First, we confirmed that the antibody specifically recognized hydroxylated FoxO3 peptide (residues 420–444) at Pro437 but not at a nearby Pro426 or non-hydroxylated FoxO3 peptide (Supplemental Figure 4). Using this antibody, we detected the presence of OH-FoxO3 under normal culture conditions with 21% O_2. Treating these cells with MG132, which inhibited ubiquitin proteasomal degradation, resulted in an increase in OH-FoxO3, whereas treating cells with a combination of MG132 and the PHD enzyme inhibitor DMOG or exposing cells to 1% O_2 resulted in a decrease in OH-FoxO3 (Figure 2I).

To test the involvement of PHD isoforms in FoxO3 hydroxylation, we used siRNA technology to knock down PHD1 (>80%), PHD2 (>80%), or PHD3 (>60%) in renal epithelial cells cultured under 21% O_2 and measured OH-FoxO3 protein levels 72 hours after transfection with siRNA reagents. The results showed a significant reduction of OH-FoxO3 protein levels when PHD1, PHD2, or PHD3 was knocked down (Figure 2J). Our results con-

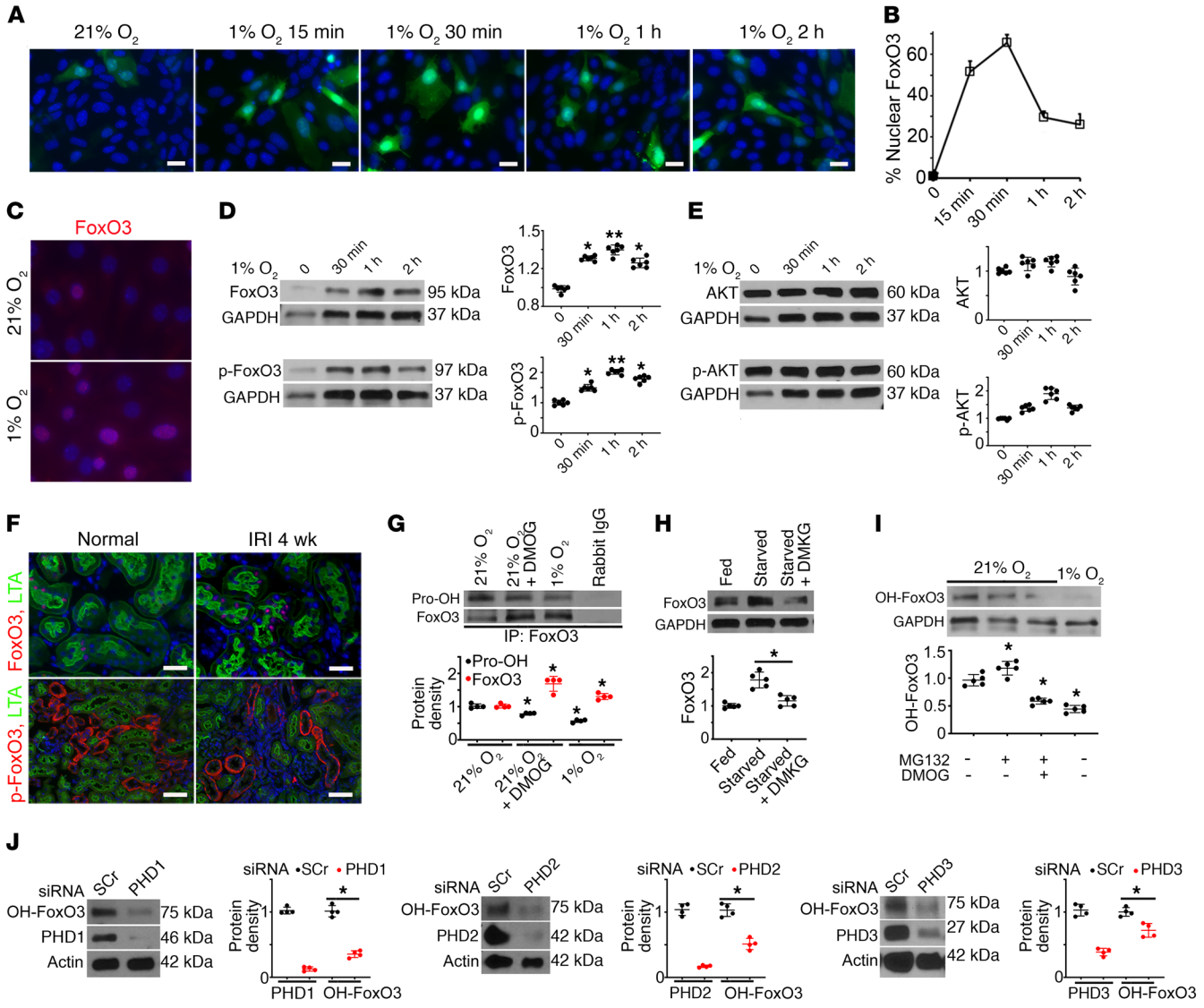

Figure 2. Hypoxia inhibits FoxO3 prolyl hydroxylation and its degradation. (**A**–**B**) Exposure of primary cultures of renal epithelial cells infected with adeno-FoxO3-GFP to 1% O_2 induced nuclear accumulation of FoxO3. (**C**) Immunostaining of endogenous FoxO3 (without overexpression) showed abundant nuclear FoxO3 (red) in cells exposed to 1% O_2 for 30 minutes. (**D** and **E**) Endogenous FoxO3 and p-FoxO3 (Ser253) protein levels increased in primary cultures exposure to 1% O_2, whereas no significant differences in AKT or p-AKT were detected. $n = 6$ with duplicates. $^*P < 0.05$ and $^{**}P < 0.01$ compared with 21% O_2. (**F**) Proximal tubules of the kidney (labeled by LTA in green at the brush border) had increased FoxO3 expression in the nucleus (red), but undetectable p-FoxO3 in the cytoplasm (red) 4 weeks after IRI. $n = 4$ for normal controls; $n = 5$ for 4 weeks after IRI (IRI 4 wk). (**G**) IP of proteins isolated from primary cultures with an antibody against FoxO3 followed by IB analysis with a pan-hydroxyl proline antibody showed reduced prolyl hydroxylated proteins (Pro-OH) but increased FoxO3 protein expression in cells exposed to 1% O_2 or cells grown in 21% O_2 and treated with the hypoxia mimetic DMOG, which inhibited PHD enzymes. Rabbit IgG served as a control. $n = 4$. $^*P < 0.05$ compared with cells exposed to 21% O_2 alone. (**H**) Supplementation of starved cells with DMKG, the cell-permeable analog of α-ketoglutarate, resulted in decreased FoxO3 protein abundance. $n = 5$. $^*P < 0.05$ comparing starved cells with starved cells plus DMKG. (**I**) An antibody raised against prolyl hydroxylated FoxO3 at Pro437 was used to detect OH-FoxO3 in primary cultures. OH-FoxO3 was present under 21% O_2, increased when MG132 was used to block its degradation via ubiquitin degradation pathway, and decreased when treated with the combination of MG132 and the PHD enzyme inhibitor DMOG or exposure to 1% O_2. $n = 3$ for rabbit IgG controls; $n = 5$ with duplicates for experimental conditions. $^*P < 0.05$ compared with 21% O_2. (**J**) Knockdown of PHD1 (>80%), PHD2 (>80%), or PHD3 (>60%) with siRNA resulted in a significant reduction of OH-FoxO3 proteins in primary renal epithelial cells cultured under 21% O_2 conditions. $n = 4$ with duplicates. $^*P < 0.05$ compared with cells transfected with scrambled siRNA (SCr). GAPDH served as a loading control in **D**, **E**, and **H**, and actin served as a loading control in **J**. Nuclei were counterstained with DAPI (blue) in **A**, **C**, and **F**. Scale bars: 20 μm (**A** and **C**) and 50 μm (**F**). A 2-tailed Student's *t* test was performed for **E**, **G**, and **J**. A 1-way ANOVA followed by Dunnett's post hoc test for multiple comparisons test was performed for **D**, **H**, and **I**.

firm that FoxO3 is a substrate for PHD1, as reported in mouse embryonic fibroblasts (MEFs) and cancer cell lines (18), and reveal that, in primary cultures of renal epithelial cells, FoxO3 can also be prolyl hydroxylated by PHD2 and PHD3 isoforms. As seen with the primary cultures exposed to 21% O_2 or 1% O_2 (Supplemental Figure 3), the isoform protein levels showed no significant differences between uninjured and injured kidneys 4 weeks after IRI (Supplemental Figure 5), suggesting that the availability of oxygen and factors affecting enzymatic activities play a more important role in FoxO3 hydroxylation.

HIF-1α contributes to FoxO3 activation and CKD protection. Since studies have also shown that FoxO3 can be activated by HIF-dependent pathways in a variety of cell types (20–23), we examined the role of HIF-1α in FoxO3 activation in hypoxic kidneys. We found that HIF-1α protein levels increased during the AKI-to-CKD transition period (Figure 3A). These results are in good agreement with the fact that renal hypoxia stabilizes HIF-1α and HIF-2α proteins and that these proteins act as central players in hypoxia adaptation through transcriptional activation of genes that promote cell survival and oxygen delivery (24–27). In the kidneys, HIF-1α is predominantly expressed by tubular epithelial cells, although low expression levels have been detected in the Foxd1-derived stromal cell lineages in the interstitial compartment (28–30). To test whether hypoxia-induced FoxO3 activation is dependent on HIF-1α, we took the *Pax8-rtTA* (31) and *Tet-O-Cre* (32) approach to delete HIF-1α by treating mice harboring the HIF-1α–floxed alleles (The Jackson Laboratory) with doxycycline or vehicle for 2 weeks. Cells with tubular deletion of HIF-1α and controls were designated *Hif-1a*^{tub} and *Hif-1a*^{ctl}, respectively. Deletion of HIF-1α was demonstrated by the absence of its gene at the genomic level (Supplemental Figure 6A). Primary culture cells were obtained from noninjured mouse kidneys. As expected, both *Hif-1a*^{tub} and *Hif-1a*^{ctl} cells had undetectable levels of HIF-1α under culture conditions with 21% O_2. Exposure of cells to 1% O_2 for 1 hour resulted in a robust accumulation of HIF-1α protein in *Hif-1a*^{ctl} cells. The protein also reached detectable levels in *Hif-1a*^{tub} cells, which could be due to the presence of Foxd1-derived fibroblasts in these cultures. In contrast, FoxO3 protein was present under normoxic conditions, and its levels increased further under hypoxic conditions in cells with and without HIF-1α deletion, though relatively lower levels were detected in cells with HIF-1α deletion (Figure 3B). Our results suggest that hypoxia can regulate FoxO3 protein levels in the absence of HIF-1α protein and that HIF-1α contributes to its regulation as well. Because HIF-1α is not known to interact with FoxO3 at the protein level, we measured *FoxO3* mRNA and detected increases of *FoxO3* mRNA in *Hif-1a*^{ctl} cells exposed to 1% O_2 for 10 and 30 minutes, but not with further exposure for 60 minutes. Deletion of HIF-1α attenuated hypoxia-induced increases in *FoxO3* mRNA (Figure 3C). Likewise, a control experiment with the known HIF-1–regulated gene phosphoglycerate kinase 1 (*Pgk-1*) showed gradual increases of *Pgk-1* mRNA in *Hif-1a*^{ctl} cells but not in *Hif-1a*^{tub} cells after exposure to 1% O_2 (Supplemental Figure 6B). These results indicate HIF-1α stimulation of FoxO3 at the transcriptional level.

HIF-1α was found to protect kidneys from acute ischemic and hypoxic injury when analyses were performed during the early repair phase (29, 33, 34). Here, we aimed to study the role of HIF-1α during AKI-to-CKD transition. In order to avoid mortality and be able to measure renal functional changes from the surviving kidney, mice were subjected to moderate-to-severe injury with 35 minutes of IRI to the left kidney along with right nephrectomy. We deleted HIF-1α in renal tubules from day 8 to day 21 (2 weeks total) after IRI to preserve the HIF-1α effects during the first week after IRI. As with the cell culture studies, deletion of HIF-1α led to lower nuclear FoxO3 expression in proximal tubules 4 weeks after IRI (Figure 3D), further confirming the contribution of HIF-1α to FoxO3 regulation. Analyses 4 weeks after IRI indicated higher tubular injury scores (54.3 ± 6.8 in *Hif-1a*^{tub} vs. 10.5 ± 2.4 in *Hif-1a*^{ctl}) along with higher urinary albumin and neutrophil gelatinase–associated lipcalin (NGAL) excretions in *Hif-1a*^{tub} mice (Figure 3, E–G). We observed that interstitial inflammation and fibrosis were also more severe, although no significant differences in microvascular density were detected between *Hif-1a*^{tub} and *Hif-1a*^{ctl} mice (Figure 3H). Furthermore, immunoblot (IB) analysis indicated lower levels of FoxO3 protein in *Hif-1a*^{tub} kidneys compared with levels in *Hif-1a*^{ctl} kidneys (relative protein density: 12.5 ± 4.2 in *Hif-1a*^{tub} vs. 35.6 ± 2.1 in *Hif-1a*^{ctl} kidneys). Interestingly, deletion of HIF-1α led to no significant changes in the LC3II/LC3I ratio (Figure 3I). Taken together, our results suggest that HIF-1α plays a role in the late phase of tubular repair after IRI and that its renal protection may be due to mechanisms other than autophagy.

Tubular FoxO3 deletion during AKI-to-CKD transition accelerates CKD development. To study the biological function of FoxO3 activation in the transition from AKI to CKD, we bred mice harboring floxed FoxO3 alleles (*FoxO3*$^{fl/fl}$) (35) with mice carrying *Pax8-rtTA* and *Tet-O-Cre* transgenes. Mice were given doxycycline to delete FoxO3 or given vehicle in the drinking water for 2 weeks (days 8–21) starting 1 week following IRI, after mice had recovered from the initial injury. We designated mice with tubular deletion of FoxO3 as *FoxO3*^{tub} mice and the mice without FoxO3 deletion as *FoxO3*^{ctl} mice. We found that FoxO3 protein expression from *FoxO3*^{tub} kidney lysates was significantly reduced to 16% of the expression levels in controls (Figure 4A). The incomplete deletion might be due to lower blood flow to the post-ischemic kidneys, which affected the delivery of doxycycline to induce Cre recombination. Tubular deletion of FoxO3 severely aggravated tubular damage 4 weeks after IRI as indicated by significantly higher injury scores, with a loss of proximal tubular brush borders, tubular cast formation, and atrophy (229 ± 5.3 vs. 22 ± 3.6 in *FoxO3*^{ctl} mice, n = 5) (Figures 4B). Tubular dilation was also more pronounced (Supplemental Figure 7). Interestingly, chronic hypoxic injury did not result in significant proliferation in the tubules located in the cortex and outer medulla in *FoxO3*^{ctl} mice, as only 2.63 ± 0.54 cells per field under ×200 magnification were found to express Ki67 compared with 2.23 ± 0.09 cells per field in normal kidneys. FoxO3 deletion doubled the number of proliferating tubular cells (4.53 ± 0.6 cells per field) and led to higher expression of the proximal tubular injury marker Kim1 (Figure 4B). Urinary NGAL excretion was 4-fold higher when FoxO3 was deleted. Additionally, urinary albumin excretion was increased in *FoxO3*^{tub} mice (53.2 ± 3.1 mg/g vs. 18.4 ± 4.1 mg/g in *FoxO3*^{ctl} mice). Serum creatinine, a frequently used but insensitive measurement of the kidney filtration function, was also significantly higher (Figure 4, C–E). Taken together, FoxO3 deletion resulted in a more severe

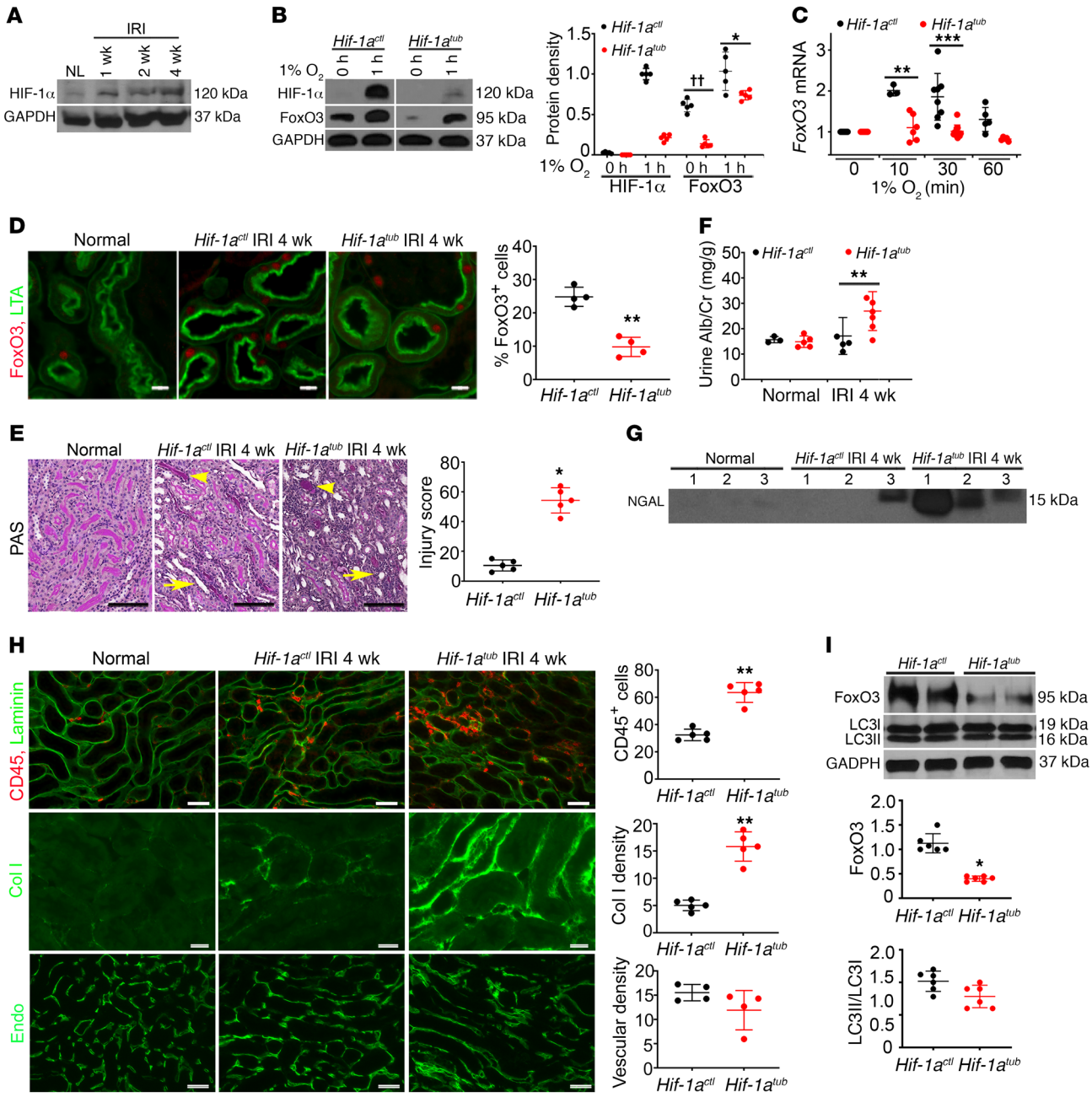

Figure 3. HIF-1α contributes to FoxO3 activation and CKD protection. (**A**) HIF-1α protein levels increased during CKD development. *n* = 4. (**B**–**C**) HIF-1α was deleted using the *Pax8-rtTA* and *Tet-O-Cre* system by giving mice doxycycline for 2 weeks prior to primary culture (*Hif-1a*^{tub}). Vehicle-treated mice (*Hif-1a*^{ctl}) were used as controls. (**B**) The hypoxia-induced increase in FoxO3 protein was partially dependent on HIF-1α in primary cultures. *n* = 5 with duplicates. $^{\dagger\dagger}P < 0.01$ and $^{*}P < 0.05$ comparing *Hif-1a*^{tub} with *Hif-1a*^{ctl} at 0 hours and 1 hour, respectively. (**C**) HIF-1α deletion abolished the increase in *FoxO3* mRNA in response to hypoxia with 1% O_2. *n* = 3–8 with duplicates. $^{**}P < 0.01$ and $^{***}P < 0.001$ compared with cells prior to exposure to 1% O_2 (0 min) in the *Hif-1a*^{ctl} or *Hif-1a*^{tub} group. (**D**) Nuclear expression of FoxO3 (red) was higher in proximal tubules (labeled with LTA in green) of *Hif-1a*^{ctl} kidneys 4 weeks after IRI. *n* = 4. $^{**}P < 0.01$. (**E**–**I**) Tubular HIF-1α was deleted from day 8 to day 21 following a 35-minute left IRI and right nephrectomy, and kidneys were analyzed 4 weeks after IRI. Tubular deletion of HIF-1α led to more severe tubular atrophy (arrowheads) and cast formation (arrows) (**E**, PAS staining, *n* = 5), higher urinary albumin and creatinine (Alb/Cr) levels (**F**, *n* = 3 or 5 for normal controls; *n* = 5 or 6 for 4 weeks after IRI), higher urinary NGAL excretion (**G**, *n* = 3 or 5 for normal controls; *n* = 5 or 6 for 4 weeks after IRI), and more interstitial inflammation and fibrosis (**H**). For the images in **H**, the top panel shows more infiltrating CD45-expressing leukocytes (red, *n* = 5), the middle panel shows more fibrosis with collagen I (Col I) deposition (green, *n* = 5), and the bottom panel shows no significant differences in the density of capillaries labeled with endomucin (green, *n* = 4) compared with *Hif-1a*^{ctl} kidneys. (**I**) Blots show lower levels of FoxO3 protein in *Hif-1a*^{tub} kidneys compared with levels in *Hif-1a*^{ctl} kidneys, but no significant difference in the LC3II/LC3I ratio was detected. *n* = 6. $^{*}P < 0.05$ and $^{**}P < 0.01$, comparing *Hif-1a*^{tub} with *Hif-1a*^{ctl} (**E**, **F**, **H**, and **I**). Scale bars: 100 μm (**E**), 50 μm (top and bottom panels of **H**), and 20 μm (**D** and middle panel of **H**). Statistical significance was determined by 2-tailed Student's *t* test (**B**, **D**, **F**, **H**, and **I**), Wilcoxon-Mann-Whitney *U* test (**E**), and 1-way ANOVA followed by Dunnett's post hoc test for multiple comparisons (**C**).

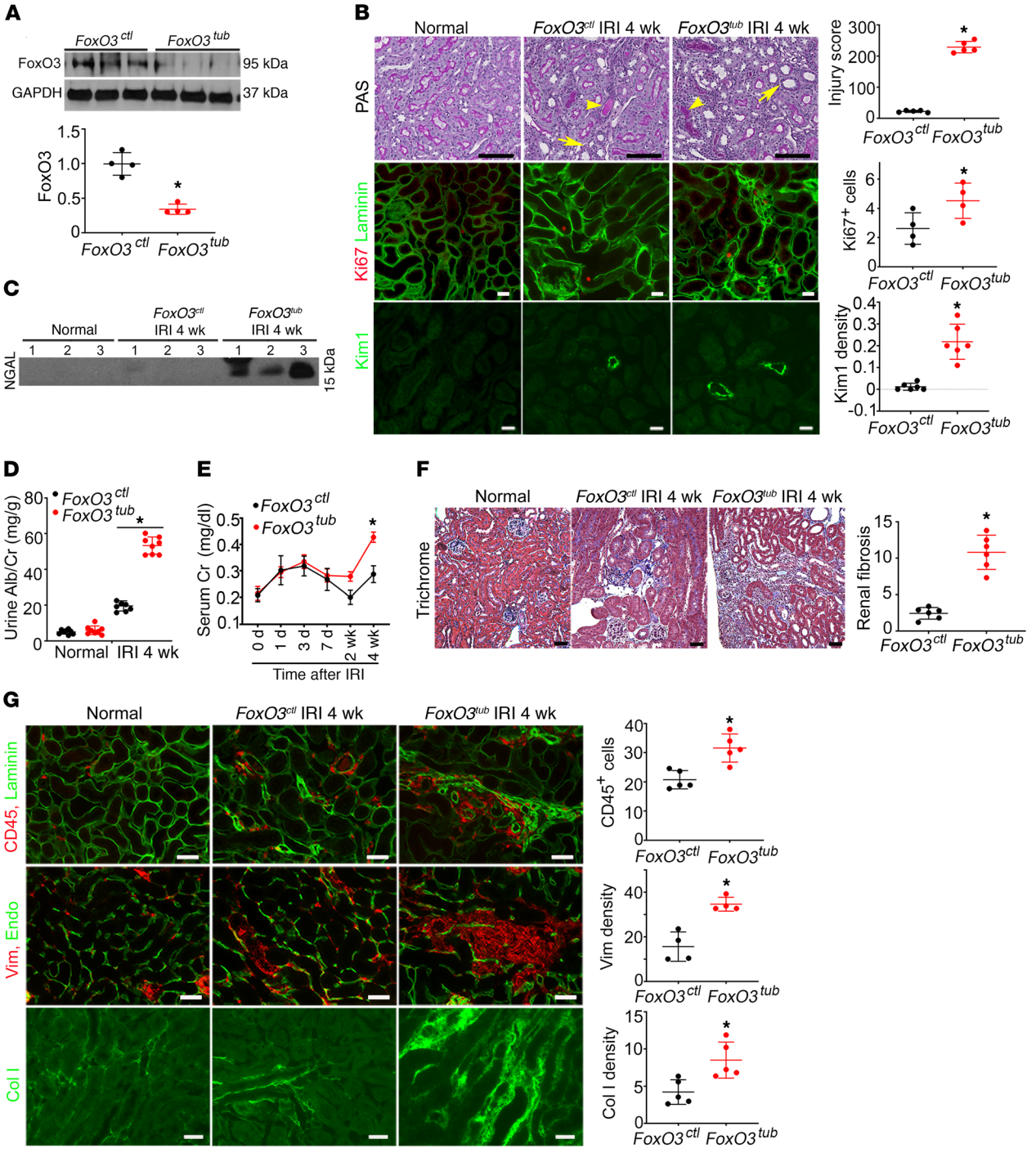

Figure 4. Tubular FoxO3 deletion during the AKI-to-CKD transition accelerates CKD development. Tubular FoxO3 was deleted from day 8 to day 21 following a 35-minute left kidney IRI and right nephrectomy. Kidneys were analyzed 4 weeks after IRI. *FoxO3*^{tub} indicates FoxO3 deletion with doxycycline treatment and *FoxO3*^{ctl} indicates control with vehicle treatment. (**A**) The *Pax8-rtTA* and *Tet-O-Cre* system led to a dramatic reduction of FoxO3 protein levels in kidney lysates. $n = 4$. (**B**) More severe tubular injury was observed in *FoxO3*^{tub} mice compared with *FoxO3*^{ctl} mice (PAS staining, $n = 5$). Arrows denote tubular atrophy, and arrowheads indicate cast formation. No increased proliferation (Ki67 expression, red) in tubules (labeled with laminin in green) was detected 4 weeks after IRI in mice without FoxO3 deletion (*FoxO3*^{ctl}) compared with normal kidneys. However, tubular Ki67 expression increased in FoxO3-deleted (*FoxO3*^{tub}) mice compared with expression levels in FoxO3-undeleted mice (*FoxO3*^{ctl}). $n = 4$. Kim 1 expression (green) also indicated more severe proximal tubular injury in *FoxO3*^{tub} mice. $n = 6$. (**C**–**E**) Increases in urinary NGAL (**C**), albumin excretion (**D**), and serum creatinine (**E**) with FoxO3 deletion (*FoxO3*^{tub}) were observed. $n = 8$. (**F**) Trichrome staining ($n = 6$) indicated more interstitial fibrosis with FoxO3 deletion (*FoxO3*^{tub}). (**G**) Deletion of FoxO3 (labeled with laminin in green) led to more severe interstitial inflammation with infiltration of CD45-expressing cells (red, $n = 5$), interstitial fibrosis with vimentin (Vim) expression (red, $n = 4$), and collagen I deposition (green, $n = 5$). The differences in the density of microvessels labeled with endomucin (green) did not reach statistical significance. Scale bars: 50 μm (B, F, and G, top 2 panels) and 20 μm (**G**, bottom panel). *$P < 0.05$ comparing *FoxO3*^{tub} with *FoxO3*^{ctl}. Statistical significance was determined by 2-tailed Student's *t* test (**A** and **B**, for Ki67 and Kim1, and **D**, **E**, and **G**) and Wilcoxon-Mann-Whitney *U* test (**B** and **F**).

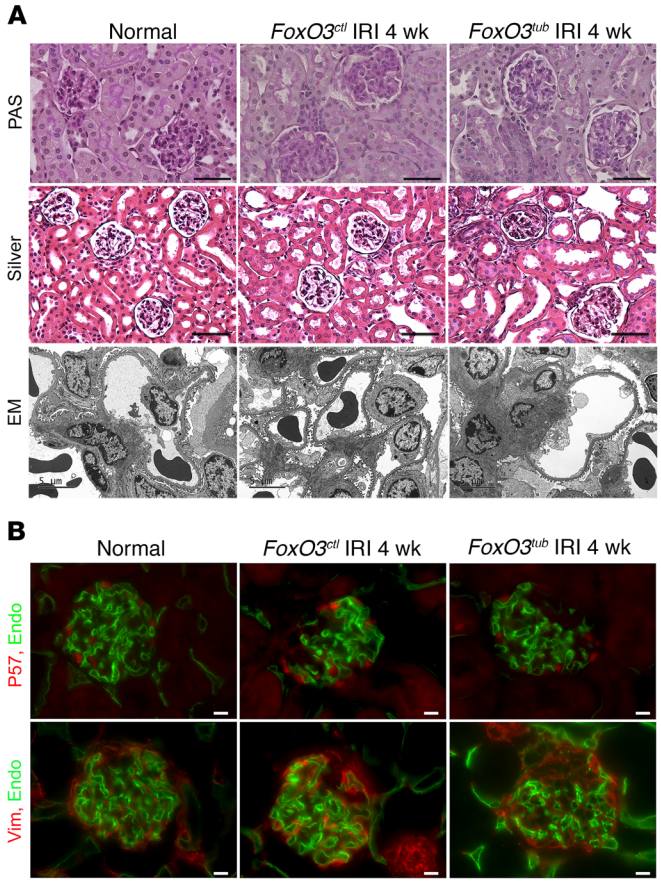

Figure 5. Tubular deletion of FoxO3 (*FoxO3^{tub}*) during the AKI-to-CKD transition results in focal glomerular sclerosis. Tubular FoxO3 was deleted from day 8 to day 21 following a 35-minute left kidney IRI and right nephrectomy, and kidneys were analyzed 4 weeks after IRI. (**A**) PAS staining indicated no increases in glomerular cellularity, and Silver staining showed mild thickening of the basement membrane in Bowman's capsule but no changes in the basement membrane of capillary loops in the glomeruli of *FoxO3^{tub}* or *FoxO3^{ctl}* mice. EM analysis showed rare podocyte foot process effacement, although more mesangial deposits were observed in *FoxO3^{tub}* kidneys. (**B**) Immunostaining of podocytes with P57 (red) showed that in *FoxO3^{tub}* and *FoxO3^{ctl}* mice, there were no significant changes in the number of podocytes per glomerulus after IRI. Top panel: Endomucin (green) labeled glomerular capillary loops. Bottom panel: Vimentin (red) and endomucin (green) staining showed focal glomerular sclerosis with vimentin deposition and loss of capillary loops in *FoxO3^{tub}* mice. $n = 4$. Scale bars: 50 μm (**A**, top and middle panels), 10 μm (**B**), and 5 μm (**A**, bottom panel).

tubular injury that triggered proliferation. However, we observed more progressive injury and incomplete tubular repair manifested with worse renal morphology and function when tubular FoxO3 was deleted.

Tubular injury is known to cause interstitial inflammation and fibrosis (5). We found that tubular injury as a result of FoxO3 deletion was accompanied by more CD45$^+$ leukocyte infiltration and more fibrotic changes, as demonstrated by trichrome staining and deposition of collagen I and vimentin in the interstitial compartment. The difference in microvascular density did not reach statistical significance (Figure 4, F and G). An additional method of evaluating fibrosis with Picrosirius red staining also indicated more fibrosis under polarized light (Supplemental Figure 8). Overall, the degree of renal structural injury and functional decline was much greater in mice with FoxO3 deletion than in those with HIF-1α deletion (tubular injury score: 229 ± 5.3 with FoxO3 deletion vs. 54.3 ± 6.8 with HIF-1α deletion), despite the similarity of endothelial rarefaction in the injured kidneys. Our results suggest that FoxO3 may play a more important role in preventing AKI-to-CKD transition and may therefore represent a better potential pathway to target to prevent or slow down CKD development.

Unlike most cases of primary glomerular disease, glomeruli at 4 weeks after IRI showed no apparent increase in cellularity in kidneys with and without tubular FoxO3 deletion. Silver staining showed a mild thickening of the basement membrane in Bowman's capsule but not the basement membrane of capillary loops in glomeruli trapped in the fibrotic region. Podocyte foot process effacement was rarely detected, although we observed more mesangial deposits in *FoxO3^{tub}* kidneys (Figure 5A). Immunostaining for P57, a marker that identifies podocytes (36, 37), showed no significant changes in the number of podocytes per glomerulus 4 weeks after IRI (9.1± 0.8 in normal mice and 7.5 ± 1.9 in *FoxO3^{tub}* and 7.2 ± 0.7 in *FoxO3^{ctl}* mice). In concordance with the electron microscopic (EM) findings, 52% of glomeruli in *FoxO3^{tub}* kidneys showed increased vimentin deposition, with focal areas showing loss of capillary loops, whereas *FoxO3^{ctl}* kidneys had milder glomerular changes, with 15% of glomeruli affected (Figure 5B). Since the *Pax8-rtTA* system is not active in podocytes (31), our results indicate a secondary glomerular response from the loss of FoxO3 protection in tubules, which could also contribute to increased urinary albumin excretion (shown in Figure 4). Similarly, analysis of glomeruli in *Hif-1a^{tub}* and *Hif-1a^{ctl}* kidneys with periodic acid–Schiff (PAS) staining and immunostaining for P57 and vimentin also showed no differences 4 weeks after IRI (Supplemental Figure 9).

Loss of FoxO3 results in reduced autophagic adaptation. To examine whether the renal protection in mice with intact FoxO3 was also associated with autophagy, we performed EM examination, which remains the gold standard for detection of autophagic vesicles. Autophagosomes and autolysosomes were more frequently observed in tubules 4 weeks after IRI (Figure 6A). In comparison, no autophagic vesicles were easily detectable in uninjured tubules (data not shown). Next, we deleted FoxO3 from tubules during the AKI-to-CKD transition period (days 8–21). As predicted, we found that autophagic levels estimated by the LC3II/LC3I ratio were reduced in *FoxO3^{tub}* kidneys. Bnip3 protein levels, a known target of FoxO3 and a key component in the autophagic machinery, were decreased as well, although ULK protein, which was essential to the initial event of autophagic activation, showed no significant changes (Figure 6B). To complement the in vivo findings, we exposed primary cultures isolated from uninjured kidneys to 1% O_2 for 30 minutes. Although *FoxO3^{ctl}* cells showed a significant increase in the LC3II/LC3I ratio compared with that of cells exposed to 21% O_2, *FoxO3^{tub}* cells had an insignificant increase in the LC3II/LC3I ratio (Supplemental Figure 10). When the autophagy reporter *CREL* mice (12) were bred with *FoxO3^{tub}* and *FoxO3^{ctl}* mice and subjected to IRI, we noted that fewer red fluorescent protein (RFP) dots were present in renal tubules when FoxO3 was

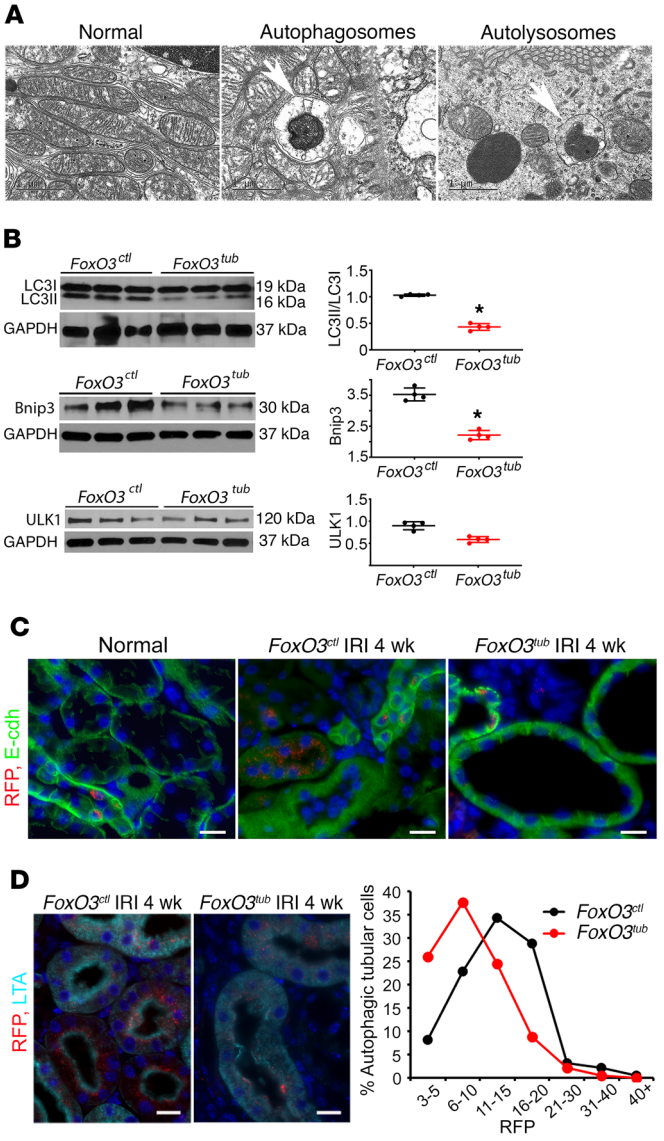

Figure 6. Loss of FoxO3 results in reduced autophagic adaptation. Tubular FoxO3 was deleted from day 8 to day 21 following a 35-minute left kidney IRI and right nephrectomy. Kidneys were analyzed 4 weeks after IRI. (**A**) Representative EM images of autophagosomes and autolysosomes (white arrows) in tubules of *FoxO3*^{ctl} mice 4 weeks after IRI. (**B**) Lower levels of LC3II, LC3I, and Bnip3 proteins were detected, but no significant changes in ULK1 protein levels were seen in *FoxO3*^{tub} kidneys ($n = 4$). *$P < 0.05$ comparing *FoxO3*^{tub} with *FoxO3*^{ctl}, by 2-tailed Student's *t* test. (**C**) The autophagy reporter *CREL* mice were bred with *FoxO3*^{tub} and *FoxO3*^{ctl} mice and subjected to IRI, as above. Fewer RFP dots were visible in renal tubules labeled with E-cadherin (green) that appeared atrophic in *FoxO3*^{tub} mice. Tubules in *FoxO3*^{ctl} mice contained a greater abundance of RFP dots. (**D**) Quantification of RFP dots in proximal tubules (labeled in cyan with LTA) indicated that the majority of autophagic cells in *FoxO3*^{tub} kidneys contained 10 or fewer dots per cell, whereas the majority of autophagic cells in *FoxO3*^{ctl} kidneys contained 10 or more dots per cell. Nuclei were counterstained with DAPI in blue in **C** and **D**. Scale bars: 20 μm (**C** and **D**).

deleted. These tubules with decreased autophagic dots appeared atrophic. In contrast, the tubules of *FoxO3*^{ctl} mice contained a greater abundance of RFP dots, and renal tubules appeared less atrophic (Figure 6C), suggesting that FoxO3 stimulates autophagy to maintain tubular homeostasis. Quantification of RFP dots in proximal tubules indicated that the majority of autophagic cells in *FoxO3*^{tub} kidneys contained 10 or fewer dots per cell. In comparison, more than 70% of autophagic cells in *FoxO3*^{ctl} kidneys contained 10 or more dots per cell (Figure 6D). These results are in a good agreement with our previous finding that FoxO3 activation increases autophagic capacity in tubules injured by urinary tract obstruction (11).

Loss of FoxO3 results in more oxidative injury. FoxO3 is a stress-responsive gene, and its targets also include molecules responsible for the control of oxidative stress (38). Renal hypoxia has been shown to increase the production of ROS, resulting in oxidative injury (39–41). We measured SOD2, a mitochondrial scavenging enzyme that is inducible by FoxO3 and plays a critical role in ROS clearance (38). We detected a significantly lower level of SOD2 protein in *FoxO3*^{tub} kidneys 4 weeks after IRI (relative protein density: 0.65 ± 0.04 vs. 1.13 ± 0.02 level in *FoxO3*^{ctl} mice) (Figure 7A). Mitochondrial superoxide levels in live cells from primary cultures isolated from *FoxO3*^{tub} kidneys showed a higher intensity of the fluorogenic dye MitoSOX Red compared with that seen in the FoxO3-undeleted cells after exposure to 1% O_2 for 1 hour. Similarly, incubating cells with dihydroethidium (DHE), a substance that could be oxidized by intracellular ROS and emit red fluorescent signals in the nuclei, showed that nearly 100% of cells isolated from *FoxO3*^{tub} kidneys emitted red nuclear signals compared with 49.6% of cells isolated from *FoxO3*^{ctl} kidneys. DHE staining of kidneys 4 weeks after IRI also indicated stronger nuclear oxidative stress in *FoxO3*^{tub} kidneys (Figure 7B). Furthermore, EM studies showed dramatic mitochondrial swelling with a loss of cristae. In *FoxO3*^{tub} cells, we detected frequent ruptures of mitochondrial inner and outer membranes (Figure 7C), which could lead to leakage of ROS to the cytoplasm and cause oxidative injury. Taken together, our results indicate an antioxidant effect of FoxO3 in preventing tubular damage. Future in-depth studies designed to effectively reduce or remove ROS in renal tubules will delineate the functional significance of the FoxO3/ROS pathway in CKD development.

FoxO3 is activated in injured tubules of human kidneys. To investigate a possible involvement of hypoxia-induced FoxO3 activation in human AKI (2 patients) or AKI on CKD (10 patients), we examined the renal microvasculature and nuclear FoxO3 expression in all 12 kidney biopsy samples taken for renal ischemia or hypoperfusion due to renal atheroembolization, volume depletion, congestive heart failure, respiratory failure, or hepatorenal syndrome. Five controls that had no specific pathological alterations were obtained from biopsies for microscopic hematuria or subnephrotic range proteinuria (Table 1). Representative images showed diminished expression of the endothelial marker CD31 in injured kidneys, in which acute tubular damage, chronic tubular changes with atrophy, and cast formation were apparent. Nuclear FoxO3 was mainly localized in the distal nephron in the control samples, but increased expression of the protein was observed in the injured proximal tubules that exhibited flat epithelia and denuded basement membranes. Furthermore, EM examination showed mitochondrial swelling with a loss of cristae as well as the presence of autophagosomes and autolysosomes in the injured kidneys (Figure 8). These results suggest a correlation between the loss of renal microvasculature and FoxO3

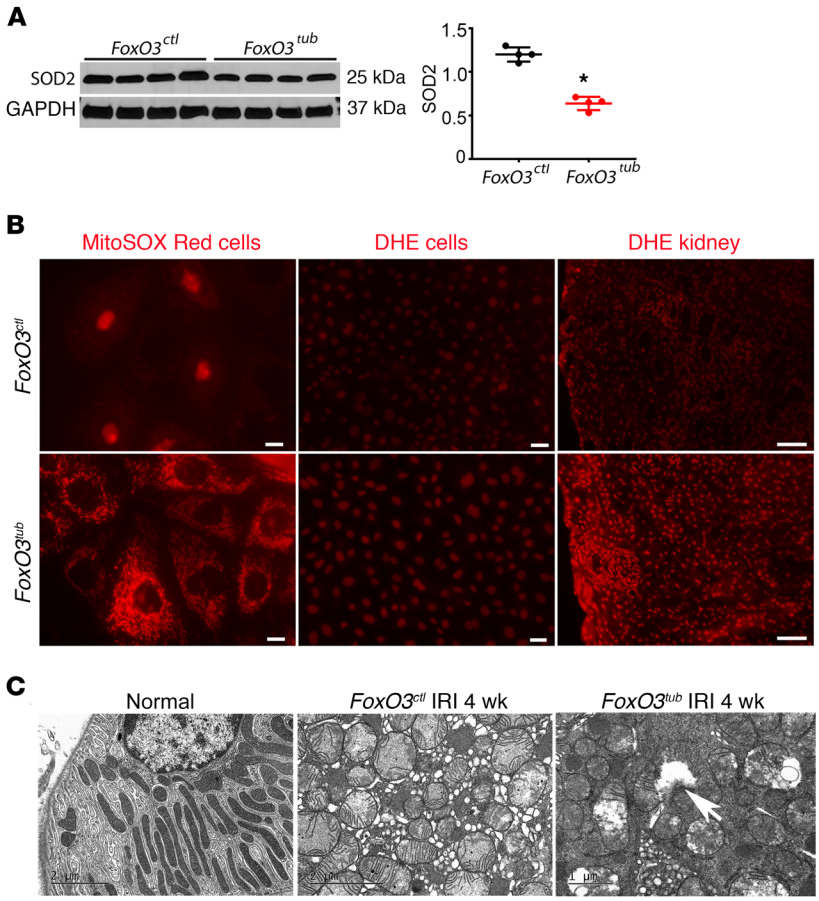

Figure 7. Loss of FoxO3 results in more severe oxidative injury. (**A**) Tubular FoxO3 was deleted from day 8 to day 21 following a 35-minute left kidney IRI and right nephrectomy. Kidneys were analyzed 4 weeks after IRI. Lower levels of SOD2 protein were detected in *FoxO3*^{tub} compared with levels in *FoxO3*^{ctl} mouse kidneys. $n = 4$. $^*P < 0.05$, comparing *FoxO3*^{tub} with *FoxO3*^{ctl}; 2-tailed Student's *t* test (**B**) Left and middle panels: Primary cultures were isolated from normal kidneys of mice treated with doxycycline or vehicle for 2 weeks (*FoxO3*^{tub} or *FoxO3*^{ctl} mice) and exposed to 1% O_2 for 1 hour prior to incubation with MitoSOX Red or DHE. Mitochondrial superoxide levels indicated by MitoSOX Red (left panel) showed higher intensity in *FoxO3*^{tub} cells. DHE (middle panel) showed that nearly 100% of *FoxO3*^{tub} cells emitted red nuclear signals compared with 49.6% in *FoxO3*^{ctl} cells. Right panel: DHE staining of the kidney showed stronger nuclear oxidative stress in *FoxO3*^{tub} kidneys 4 weeks after IRI. (**C**) EM images show dramatic mitochondrial swelling with a loss of cristae in epithelial cells 4 weeks after IRI. In *FoxO3*^{tub} cells, frequent ruptures of mitochondrial inner and outer membranes were detected (white arrow). Scale bars: 10 μm (left panel in **B**), 50 μm (middle panel in **B**), and 100 μm (right panel in **B**); 2 μm (left and middle panels in **C**) and 1 μm (right panel in **C**).

activation in human AKI or AKI on CKD and further highlight the significance of FoxO3 activation in tubular stress response.

In summary, our study indicates that chronic hypoxia, which is an important pathogenic factor for CKD development, can activate FoxO3 via inhibition of its prolyl hydroxylation and degradation in a manner similar to HIF regulation by PHD enzymes. HIF-1α contributes to hypoxia-mediated activation of FoxO3, which plays an important role in counteracting the detrimental effects of hypoxia by increasing autophagy and decreasing oxidative stress (Figure 9). Further research and discoveries related to the stimulation of FoxO3-mediated responses that ameliorate hypoxia-induced stress and injury may provide a basis for therapies to prevent or slow down the development of CKD.

Discussion

We demonstrate that the transcription factor FoxO3 regulates adaptive responses that counteract adverse effects of chronic hypoxia in the kidney through increased autophagy and reduced oxidative stress. Unlike extensive cell death and cell proliferation after abrupt cessation of blood flow and oxygen supply, chronic hypoxia does not lead to a dramatic increase in tubular proliferation as a repair mechanism 4 weeks after IRI. On the other hand, autophagy, which is an evolutionarily conserved mechanism for cell survival, can be activated during acute renal IRI (12) or with chronic hypoxia and metabolic perturbations (11). Signals for autophagy induction can be transduced to the nutrient and energy sensors that include AMPK, mTORC1, and NADH-dependent deacetylases of the sirtuin family, as well as other molecular pathways that involve stress responses (42, 43). FoxO3 is 1 of the 4 mammalian FoxO transcription factors that include FoxO1, FoxO3, FoxO4, and FoxO6 (44–47). FoxO3 has been studied most extensively and has been shown to modulate stress responses, metabolism, autophagy, apoptosis, and cell differentiation (48, 49). FoxO3 activity is largely regulated by posttranslational mechanisms that include phosphorylation, acetylation, and ubiquitination (49–51). In the presence of survival factors, such as growth factors and nutrients, FoxO3 is phosphorylated, predominantly by AKT, and translocated to the cytoplasm, where it is degraded by the ubiquitin proteasomal system. In contrast, under stress conditions, FoxO3 accumulates in the nucleus and functions as either a transcription activator or repressor, in a context-dependent fashion, to regulate adaptive responses (48, 49).

Recent identification of FoxO3 as a novel substrate for the PHD1 enzyme (18) has led to our current understanding of the mechanism of hypoxia-induced FoxO3 activation in the kidney. Of the 3 PHD enzymes that function as oxygen sensors, PHD2 is the primary PHD for the α subunit of the HIF proteins (52, 53), while PHD1 and PHD3 may play additional roles beyond regulating HIF proteins (23, 54). Using decarboxylation assays to screen 1,000 proteins that could potentially be hydroxylated by PHD1 in vitro, Zheng et al. demonstrated that FoxO3 was hydroxylated at Pro426 and Pro437, which disrupted the binding with USP9x deubiquitinase, thereby promoting FoxO3 degradation via the ubiquitin proteasomal system (UPS). Prolyl hydroxylation was confirmed in a breast cancer cell line and in 293 embryonic kidney cells (18). The recent development of an antibody raised specifically against hydroxyl Pro437 in FoxO3 has allowed us to detect endogenous prolyl hydroxylated FoxO3 in renal tubular epithelial cells. Furthermore, UPS inhibition with MG132 increases but hypoxia reduces OH-FoxO3 (Pro437) protein levels, confirming that prolyl hydroxylation and proteasomal degradation are mechanisms that regu-

Table 1. Characteristics of human kidney biopsies

	Controls, *n* = 5	Kidney injuries, *n* = 12
Age range (yr)	25–74 (51.0 ± 19.4)	50–81 (68.2 ± 8.5)
Baseline SCr (mg/dl)	N/A	0.7–2.1 (1.7 ± 0.5)
SCr at biopsy (mg/dl)	0.81–1.0 (0.9 ± 0.1)	1.6–9.4 (4.4 ± 2.1)
Biopsy indications	Microscopic hematuria	
Subnephrotic proteinuria	Kidney ischemia or hypoperfusion[A]	
Biopsy findings (no. of patients)	No specific pathologic alterations (5 of 5)	Acute tubular injury (12 of 12); chronic renal disease (*n* = 10) with focal (8 of 10) or diffuse (2 of 10) tubular atrophy and interstitial fibrosis[B]

[A]A total of 12 renal biopsy samples were obtained from patients with kidney ischemia or hypoperfusion due to renal atheroembolization (*n* = 5), volume depletion (*n* = 2), congestive heart failure (*n* = 2), respiratory failure (*n* = 2), or hepatorenal syndrome (*n* = 1). [B]Focal <50% and diffuse, ≥50% of tubular atrophy and interstitial fibrosis. Values are expressed as the mean ± SD. SCr, serum creatinine.

late FoxO3 protein abundance. Interestingly, we also show that the levels of p-FoxO3 at Ser253 increased when primary cultures of renal epithelia cells were exposed to hypoxic conditions. The same culture conditions did not increase AKT or p-AKT protein levels significantly, suggesting that higher levels of p-FoxO3 are more likely a result of decreased degradation rather than increased formation. At present, it is unclear whether p-FoxO3 can also be prolyl hydroxylated or FoxO3 prolyl hydroxylation facilitates the degradation. Future biochemical studies will need to address the relationship among posttranslational modifications.

It is interesting to note that the hydroxylase activity shared by PHD isoforms is not unique to FoxO3, because all 3 isoforms have also been shown to hydroxylate synthetic HIF-1α peptides in vitro (55–57) and HIF-1 α proteins in cells expressing high levels of isoforms (58). Indeed, in vitro and animal studies have suggested that PHD2 is the main hydroxylase for HIF (52, 53, 58). It is possible that the level and pattern of the enzyme expression as well as conditions affecting the enzymatic activity could influence substrate preference and product formation in a cell-type– and context-dependent manner. At this time, the selectivity and relative contribution of the isozyme to HIF and FoxO3 regulation during CKD development are not known. Future studies involving the selective inhibition or deletion of the individual isoform in renal tubules will help address this important question.

We have previously shown that persistent obstructive injury to the kidney leads to FoxO3 activation, which increases the formation of autophagosomes. FoxO3 activation increases the expression of core Atg proteins including ULK1, Beclin-1, Atg9A, Atg4B, and Bnip3 in kidneys to sustain the autophagic response in obstructed kidneys (11). This study shows that after IRI, FoxO3 is progressively activated in the hypoxic tubular cells to stimulate autophagy. Using an antibody against LC3B, we demonstrated increased conversion of LC3I to LC3II, which is a commonly used method to evaluate autophagy. It is important to note that LC3 proteins, such as microtubule-associated protein 1 light chain 3 α (LC3α) plays a crucial role in LC3-associated phagocytosis (LAP) (59–61). The *CREL* mouse has not been thoroughly studied as a valuable model for assessing LAP, which may occur in the kidneys with hypoxia and inflammation.

FoxO3 activation reduces oxidative stress and injury by increasing mitochondrial SOD2 expression. In HeLa cells, FoxO3 has been shown to be activated by hypoxia to represses a set of nuclear-encoded mitochondrial genes to reduce oxygen consumption (21). It is conceivable that metabolic adaptation, combined with a reduction in ROS formation, promotes cell survival under hypoxic conditions. However, prolonged and escalating stress input may exceed compensatory mechanism of FoxO3 activation, leading to eventual CKD. This is supported by the fact that ROS-induced stress signals were reduced but not absent in FoxO3-competent renal tubular cells, as the oxidative injury and cell death that have recently been referred to as ferroptosis (62–64) could also be induced by ROS generated from organelles other than the mitochondria (65).

In this study, we found that tubular deletion of FoxO3 led to much more profound renal injury than did tubular deletion of HIF-1α (tubular injury score: 229 ± 5.3 vs. 54.3 ± 6.8). In addition, FoxO3 was expressed in hypoxic kidneys as well as in normal kidneys when HIF-1α protein was not easily detectable. These results suggest a pleiotropic effect of FoxO3 in renal hemostasis and stress adaptation. Further studies of the effects of FoxO3 on other CKD pathogenic factors such as cell death, immune response, interstitial inflammation, and fibrosis will provide a biological basis for targeting FoxO3 as a potential therapeutic approach for CKD. Our current study cannot rule out possible contributions to renal protection by other FoxO members that may have overlapping functions. For example, FoxO1, which is highly expressed in insulin-responsive tissues, can orchestrate the transcriptional networks, thereby regulating glucose and lipid metabolism (66). However, FoxO1 is not consistently elevated in response to hypoxia (18, 21, 67). Future studies manipulating FoxO1 alone or in combination with FoxO3 may shed light on a possible role of FoxO1 in CKD.

Molecular oxygen is essential to mitochondrial energy metabolism and numerous chemical reactions and activities. The VHL/PHD/HIF pathway is the best-characterized O_2-sensing system to date. This pathway regulates a large molecular network required for adaptation to low oxygen by increasing the expression of hundreds of genes involved in diverse cellular functions. HIF-1 protein is critical for rapid as well as long-term adaptations to hypoxia (68). As observed in MEFs, endothelial cells, and some other cell types (21, 22), we found that FoxO3 activation in renal tubular cells was partially dependent on HIF-1α, as deletion of HIF-1α blunted FoxO3 accumulation. HIF-1α can interact with a

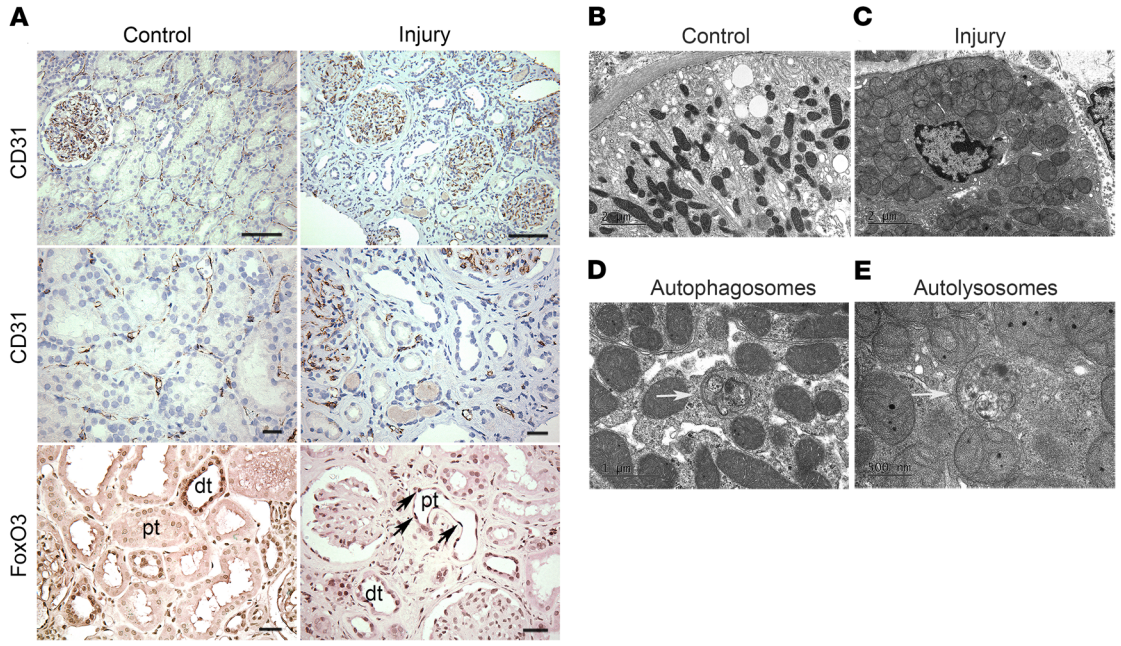

Figure 8. FoxO3 is activated in human kidneys with ischemic injury. Human kidney AKI and AKI on CKD samples were obtained from biopsies. Control samples were obtained from biopsies for microscopic hematuria or proteinuria with no specific pathologic alterations. (**A**) The endothelial marker CD31 (dark brown) in the top panel (original magnification, ×200) and middle panel (original magnification, ×400) indicated abundant peritubular capillaries in controls but diminished microvessels surrounding tubules with acute injury, atrophy, or cast formation. Nuclear expression of FoxO3 (dark brown, bottom panel) was predominantly localized in the distal tubules (dt) in controls but was increased (black arrows) in the injured proximal tubules (pt), with flat epithelia and a denuded basement membrane. (**B**–**C**) EM images showed normal mitochondria in controls but diffused mitochondrial swelling with loss of cristae in injured epithelia. (**D** and **E**) EM analysis detected autophagosomes and autolysosomes (white arrow) in the epithelia of injured kidneys. Scale bars: 50 μm (**A**); 2 μm (**B**–**C**); 1 μm and 500 nm (**E**).

large number of proteins to regulate protein stability, but it is not known to interact with FoxO3 at the protein-protein level (69). In the promoter regions of the human and murine FoxO3 genes, there are 9 conserved hypoxia response elements (HREs). This suggests that HIF-1 may activate the FoxO3 promoter to increase its transcription, as shown in our studies and in studies involving MEFs and NIH3T3 cells (20). However, FoxO3 protein was present under normoxic conditions when HIF-1α protein was barely detectable. Furthermore, HIF-1α deletion prevented a hypoxia-induced increase in *FoxO3* mRNA to a significant degree but did not prevent an increase in FoxO3 protein abundance completely, confirming that HIF-1α could function as a transcriptional regulator for FoxO3 and that hypoxia stabilizes existing FoxO3 protein at the posttranslational level.

HIF-1α protein levels increased in the hypoxic kidneys 1–4 weeks after IRI. Using the inducible Cre system, we selectively deleted HIF-1α in all tubular cells from day 8 to day 21, starting 1 week after the ischemic insult. This model retains the known beneficial effect of HIF-1α during the acute phase and allows the examination of HIF-1α effects during the AKI-to-CKD transition period. We show that HIF-1α–deleted kidneys had more tubular injury and interstitial fibrosis. Tubular and interstitial interdependence has been well demonstrated by elegant studies, in which direct ablation and injury to tubular cells led to interstitial fibrosis (5). At this time, the role of HIF-1α in CKD-associated fibrosis is not fully understood. Studies using different models of CKD and various pharmacological or genetic approaches to modulate HIF proteins have generated conflicting results (70). In the kidney, HIF-1α is predominantly expressed by the tubules, but a low level of expression has also been detected in Foxd1-derived cells in the interstitium (28–30). In contrast, HIF-2α is expressed in interstitial cells to regulate erythropoietin production (26, 30, 71). Although treating mice with a PHD enzyme inhibitor before ischemic injury ameliorates renal fibrosis and anemia, pharmacological inhibition of PHDs in the early phase following injury had no effect. PHD inhibitor treatment reduces the degradation of HIF-1α, HIF-2α, and probably other PHD substrates in all kidney cells and extrarenal organs, thus preventing an accurate assessment of HIF-1 function in the kidneys (33). Another study showed that selective ablation of HIF-1α in proximal tubules before obstructive injury reduces epithelial-to-mesenchymal transition (EMT) in mice with unilateral ureteral obstruction (UUO). The profibrotic effect of HIF-1 was attributed to increased migration and fibrogenic gene expression in tubular epithelia (72). Since the contribution of EMT to interstitial fibrosis may not be as significant as previously thought (73–75), progressively atrophic tubules in the UUO model could express profibrotic genes that signal interstitial cells to undergo fibrotic changes rather than provide a direct cellular source for myofibroblasts. In comparison, 35 minutes of IRI produced a mild CKD phenotype with focal and mild tubular atrophy when epithelial stress responses were intact. However, tubular deletion of FoxO3 or HIF-1α removed survival and adaptive mechanisms, leading to more severe tubular injury, which could crosstalk with interstitium and aggravate interstitial pathology.

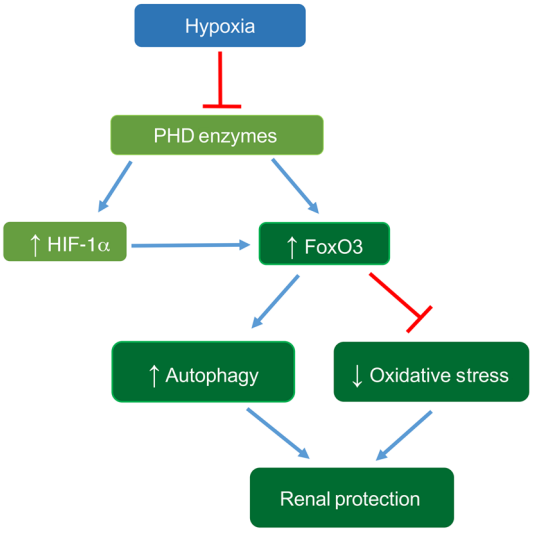

Figure 9. Proposed mechanism of hypoxia-induced FoxO3 activation, leading to renal protection. Renal hypoxia inhibits PHD enzymes and increases FoxO3 protein abundance by direct inhibition of FoxO3 degradation and via a HIF-1α–mediated mechanism. FoxO3 activation stimulates autophagy and reduces oxidative stress, thus providing renal protection during the AKI-to-CKD transition.

Therefore, our study highlights the interdependency of tubules, renal microvessels, and interstitia in maintaining kidney health and confirms the importance of taking an integrated approach to preventing CKD.

Methods

Animal studies. Methods for renal IRI in mice have been described previously (12). Briefly, 6- to 8-week-old female mice of various strains were anesthetized with isoflurane, and the left renal pedicle was clamped for 35 or 45 minutes before clamp release to allow reperfusion to the kidney. The right kidney was left intact or removed at the same time. To delete FoxO3 or HIF-1α, *Pax8-rtTA Tet-O-Cre FoxO3*$^{fl/fl}$ or *Pax8-rtTA Tet-O-Cre Hif-1a*$^{fl/fl}$ mice were given 2 mg/ml doxycycline in drinking water from day 8 to day 21 (2 weeks), starting 1 week after IRI. Vehicle-treated mice served as controls.

Tubular injury score and quantification of renal fibrosis and tubular dilation. Random images (10 photos at the outer stripe of the outer medulla [OSOM] for each kidney) of PAS-stained sections were obtained at ×20 magnification using a Zeiss Observer Z1 microscope, and ImageJ software (NIH) was used to obtain tubular injury scores. Briefly, a graticule grid was randomly placed on each picture to generate 100 grids. Histology of tubular profiles of each grid was carefully examined, and a score 0 or 1 was given for each grid: 0 = normal histology; 1 = tubular cell swelling, brush border loss, nuclear condensation, or tubular atrophy. The injury score was calculated by adding all 100 grids from each image and all 10 images from each kidney. Using this grid point counting method, renal fibrosis and tubular dilatation were quantified for kidney sections stained with Masson's trichrome.

Quantification of autophagic capacity. Images (×630 magnification) of proximal tubules identified by Lotus tetragonolobus agglutinin (LTA) staining were randomly selected. Cells that contained 3 or more RFP dots were counted as autophagic cells, and at least 100 cells were counted in each kidney. Autophagic cells were further divided into subgroups that contained 3–5, 6–10, 11–15, 16–20, 21–30, 31–40, 41–50, or more than 50 RFP dots per cell. Quantification was performed in duplicate.

Renal epithelial cell culture and analysis. Kidneys were collected from 3- to 5-week-old mice, and tubular cells were isolated for primary culture using established methods (11). For adenoviral infection, cells grown on chamber slides at 70% confluence were infected with Ad-GFP (Vector Biolabs, 1060) or Ad-GFP-FoxO3a (Vector Biolabs, 1026) at a MOI of 5 for 48 hours, then exposed to 1% O_2 in the hypoxic chamber (Biospherix, C21) for 15 minutes to 2 hours. Media for the hypoxia study were equilibrated in a 1% O_2 atmosphere overnight before use. Infected cells grown in 21% O_2 were used as controls. To quantify nuclear FoxO3 expression, cells were fixed with cold 4% paraformaldehyde (PFA) (Affymetrix, 19943 1LT) for 10 minutes, washed in PBS, and coverslipped in DAPI before imaging at ×400 magnification. To starve cells, the cells were incubated in Earle's balanced salt solution (EBSS) (MilliporeSigma, E2888) for 2 hours to deprive them of glucose and amino acids with and without 5 mM DMKG (MilliporeSigma, 34631-5G). Cells under normal culture conditions were used as controls. To delete HIF-1α, *Pax8-rtTA Tet-O-Cre Hif1α*$^{fl/fl}$ mice were treated with doxycycline in the drinking water (2 mg/ml) for 2 weeks before culturing and analysis.

Immunostaining and image analysis. Immunostaining was performed using established methods and conducted in duplicate (12). Detailed information on the staining procedures and antibodies used is provided in the Supplemental Methods. Sections were visualized with a Zeiss AxioObserver Z1 fluorescence microscope, photographed with a digital camera, and analyzed with AxioVision software.

IB and IP analyses. Tissue preparation and IB analyses were performed as previously described (76). Detailed procedures and antibody information are provided in the Supplemental Methods. IP of FoxO3 followed by IB analysis with a pan-hydroxyl proline antibody were performed with total cellular proteins from primary cultures using the Catch and Release V2.0 Reversible Immunoprecipitation System (MilliporeSigma, 17-500A). Briefly, 500 μg cellular proteins extracted with RIPA buffer were mixed with 0.1 μg FoxO3 antibody (Cell Signaling Technology, 2497), 10 μl affinity ligand, and washing buffer to 500 μl onto each column, incubated at room temperature for 1 hour, and diluted with 70 μl elution buffer denatured with 5% 2-mercaptoethanol (MilliporeSigma, M-6250). The elution was boiled at 95°C for 10 minutes and loaded at 10 μl per lane, with IB performed to detect the hydroxylation of FoxO3.

Detection of OH-FoxO3 (Pro437). The specificity of the antibody against OH-FoxO3 at Pro437 (Millipore, ABE1848) was first tested by spotting various amounts of N-terminal biotinylated FoxO3 peptides (residues 420–444) on the nitrocellulose membrane followed by detection by the antibody. An anti-biotin antibody was used to confirm the detection of FoxO3 peptides. The peptide sequences are as follows: WT FoxO3 420–444, GSGLGSPTSSFNSTVFGPSSLNSLR; FoxO3 P426-OH, GSGLGSP (OH) TSSFNSTVFGPSSLNSLR; and FoxO3 P437-OH, GSGLGSPTSSFNSTVFGP(OH)SSLNSLR. Next, renal tubular cells grown in normal culture conditions were treated with the proteasome inhibitor MG132 (10 μM, MilliporeSigma) in the presence or absence of the PHD inhibitor DMOG (1 mM, MilliporeSigma) for 2.5 hours, or with no inhibitor. Another group of cells were exposed to 1% O_2 for 1 hour. Proteins were subjected to IB analysis of OH-FoxO3 at Pro437 using the above antibody.

Superoxide detection with MitoSOX red and DHE. Renal epithelial cells grow on chamber slides were exposed to 1% O_2 for 1 hour followed by incubation with MitoSOX Red fluorescent probe (MilliporeSigma, M36008) at 5 μM or DHE (Thermo Fisher Scientific, D11347) at 0.5 μM for an additional 30 minutes in 1% O_2. Cells were rinsed with PBS, coverslipped in PBS, and examined. To measure kidney oxidative stress, freshly prepared snap-frozen sections (10-μm thick) were incubated with DHE at 1 μM in a humidified chamber at 37°C for 10 minutes in the dark before rinsing in PBS and mounting with Vectashield (Vector, H-1200-10). Sections were examined immediately, photographed at a magnification of ×200, and analyzed.

siRNA transfection. Primary cultures of renal epithelial cells grown to 60% to 80% confluence were transfected with scrambled siRNA or siRNA against PHD1, PHD2, or PHD3 (20 nM) using Lipofectamine RNAiMax reagents (Invitrogen, Thermo Fisher Scientific, 13778-150) for 72 hours before cell harvesting for Western blot analysis of PHD isoforms and OH-FoxO3 proteins. The transfection procedure and siRNA sequences are described in the Supplemental Methods.

Urine and blood analyses. Urine albumin was measured with the mouse albumin ELISA kit (Crystal Chem, 80630), and urine and serum creatinine was measure with the mouse creatinine kit (Crystal Chem, 80350) following the manufacturer's instructions. Urinary NGAL was analyzed using published methods (77, 78).

Human kidney biopsy studies. All human kidney biopsy samples were obtained from Columbia University Medical Center from 2012–2018. Five patients who underwent biopsy procedures for microscopic hematuria or subnephrotic range proteinuria but had no specific pathologic alterations were designated as the control group. Twelve patients who underwent biopsy procedures for AKI or AKI on CKD due to renal ischemia and/or hypoperfusion were designated as the injury group. Paraffin sections (3-μm thick) were used for immunohistochemical analysis of CD31 (1A10) (Leica, PA0250) followed by the refined DAB detection method using the Leica HistoCore SPECTRA system at the Anatomical Pathology and Cell Biology Core at Columbia University Medical Center, or FoxO3 (75D8) (Cell Signaling Technology, 2497, 1:50) was done with a DAB detection method. Transmission EM studies were performed using the standard method, and images were acquired with a JEOL JEM-1011 electron microscope equipped with a Gatan digital camera.

Study approval. All procedures involving mice were conducted according to the NIH's *Guide for the Care and Use of Laboratory Animals* (National Academies Press, 2011) and approved by the IACUC of Columbia University. Human kidney biopsy samples were obtained under a protocol approved by the IRB at Columbia University Medical Center and deidentified before further study.

Statistics. The number of animals or cell cultures used is indicated for each experiment. All cell cultures were performed in duplicate. Data are presented as the mean ± SEM and compared using a 2-tailed Student's *t* test to determine the statistical significance between 2 groups. Renal injury scores, tubular dilatation, and renal fibrosis (Masson's trichrome staining) for WT and mutant mice were analyzed with a nonparametric *t* test (Wilcoxon-Mann-Whitney *U*). A 1-way ANOVA followed by Dunnett's post hoc test for multiple comparisons was used to analyze study results when more than 2 groups were involved. A *P* value of less than 0.05 was considered statistically significant.

Author contributions

LL helped design and performed the majority of experiments, analyzed data, and assisted with manuscript preparation. HK performed the experiments and acquired and analyzed data. QZ validated the antibody against OH-FoxO3 at Pro437 and provided helpful discussions. QAA advised on study design and data interpretation and edited the manuscript. VDD provided expertise and insightful discussions on the pathology of human kidney biopsy samples and reviewed mouse kidney histopathology. FL designed and directed the study, performed experiments, and wrote the manuscript.

Acknowledgments

This work was supported by NIH grant R01DK107653 (to FL). We thank Julia Liu and Catherine Ha (both from the Department of Pediatrics, Columbia University) for technical assistance and Pamela Good for helpful suggestions and professional proofreading. We thank MilliporeSigma for providing the anti–OH-FoxO3 (Pro437) as a noncatalog antibody for the study and Lianxin Hu for characterization of the antibody. We thank Zhimin Yu for expert assistance with EM preparation and image acquisition.

Address correspondence to: Fangming Lin, Division of Pediatric Nephrology, Department of Pediatrics, Columbia University Vagelos College of Physicians and Surgeons, 622 West 168th Street, PH17-102F, New York, New York 10032, USA. Phone: 212.305.0793; Email: FL2300@columbia.edu.

1. Chawla LS, Eggers PW, Star RA, Kimmel PL. Acute kidney injury and chronic kidney disease as interconnected syndromes. *N Engl J Med*. 2014;371(1):58–66.
2. Coca SG, Singanamala S, Parikh CR. Chronic kidney disease after acute kidney injury: a systematic review and meta-analysis. *Kidney Int*. 2012;81(5):442–448.
3. Humphreys BD, et al. Intrinsic epithelial cells repair the kidney after injury. *Cell Stem Cell*. 2008;2(3):284–291.
4. Lin F, Moran A, Igarashi P. Intrarenal cells, not bone marrow-derived cells, are the major source for regeneration in postischemic kidney. *J Clin Invest*. 2005;115(7):1756–1764.
5. Grgic I, et al. Targeted proximal tubule injury triggers interstitial fibrosis and glomerulosclerosis. *Kidney Int*. 2012;82(2):172–183.
6. Yang L, Besschetnova TY, Brooks CR, Shah JV, Bonventre JV. Epithelial cell cycle arrest in G2/M mediates kidney fibrosis after injury. *Nat Med*. 2010;16(5):535–543, 1p following 143.
7. Zuk A, Bonventre JV. Acute Kidney Injury. *Annu Rev Med*. 2016;67:293–307.
8. Basile DP, et al. Progression after AKI: Understanding Maladaptive Repair Processes to Predict and Identify Therapeutic Treatments. *J Am Soc Nephrol*. 2016;27(3):687–697.
9. Basile DP, Donohoe D, Roethe K, Osborn JL. Renal ischemic injury results in permanent damage to peritubular capillaries and influences long-term function. *Am J Physiol Renal Physiol*. 2001;281(5):F887–F899.
10. Galluzzi L, Pietrocola F, Levine B, Kroemer G. Metabolic control of autophagy. *Cell*. 2014;159(6):1263–1276.
11. Li L, Zviti R, Ha C, Wang ZV, Hill JA, Lin F. Forkhead box O3 (FoxO3) regulates kidney tubular autophagy following urinary tract obstruction. *J Biol Chem*. 2017;292(33):13774–13783.
12. Li L, Wang ZV, Hill JA, Lin F. New autophagy reporter mice reveal dynamics of proximal tubular autophagy. *J Am Soc Nephrol*. 2014;25(2):305–315.
13. Sweeney WE, et al. Phenotypic analysis of conditionally immortalized cells isolated from the BPK model of ARPKD. *Am J Physiol, Cell Physiol*. 2001;281(5):C1695–C1705.
14. Brunet A, et al. Akt promotes cell survival by

phosphorylating and inhibiting a Forkhead transcription factor. *Cell*. 1999;96(6):857–868.
15. Biggs WH, Meisenhelder J, Hunter T, Cavenee WK, Arden KC. Protein kinase B/Akt-mediated phosphorylation promotes nuclear exclusion of the winged helix transcription factor FKHR1. *Proc Natl Acad Sci U S A*. 1999;96(13):7421–7426.
16. Brunet A, Park J, Tran H, Hu LS, Hemmings BA, Greenberg ME. Protein kinase SGK mediates survival signals by phosphorylating the forkhead transcription factor FKHRL1 (FOXO3a). *Mol Cell Biol*. 2001;21(3):952–965.
17. Plas DR, Thompson CB. Akt activation promotes degradation of tuberin and FOXO3a via the proteasome. *J Biol Chem*. 2003;278(14):12361–12366.
18. Zheng X, et al. Prolyl hydroxylation by EglN2 destabilizes FOXO3a by blocking its interaction with the USP9x deubiquitinase. *Genes Dev*. 2014;28(13):1429–1444.
19. Soilleux EJ, Turley H, Tian YM, Pugh CW, Gatter KC, Harris AL. Use of novel monoclonal antibodies to determine the expression and distribution of the hypoxia regulatory factors PHD-1, PHD-2, PHD-3 and FIH in normal and neoplastic human tissues. *Histopathology*. 2005;47(6):602–610.
20. Bakker WJ, Harris IS, Mak TW. FOXO3a is activated in response to hypoxic stress and inhibits HIF1-induced apoptosis via regulation of CITED2. *Mol Cell*. 2007;28(6):941–953.
21. Jensen KS, et al. FoxO3A promotes metabolic adaptation to hypoxia by antagonizing Myc function. *EMBO J*. 2011;30(22):4554–4570.
22. Zhang S, et al. FoxO3a modulates hypoxia stress induced oxidative stress and apoptosis in cardiac microvascular endothelial cells. *PLoS ONE*. 2013;8(11):e80342.
23. Zhang Q, et al. Control of cyclin D1 and breast tumorigenesis by the EglN2 prolyl hydroxylase. *Cancer Cell*. 2009;16(5):413–424.
24. Semenza GL. Oxygen sensing, hypoxia-inducible factors, and disease pathophysiology. *Annu Rev Pathol*. 2014;9:47–71.
25. Kaelin WG, Ratcliffe PJ. Oxygen sensing by metazoans: the central role of the HIF hydroxylase pathway. *Mol Cell*. 2008;30(4):393–402.
26. Nangaku M, Eckardt KU. Hypoxia and the HIF system in kidney disease. *J Mol Med*. 2007;85(12):1325–1330.
27. Zhang H, et al. Mitochondrial autophagy is an HIF-1-dependent adaptive metabolic response to hypoxia. *J Biol Chem*. 2008;283(16):10892–10903.
28. Rosenberger C, et al. Expression of hypoxia-inducible factor-1alpha and -2alpha in hypoxic and ischemic rat kidneys. *J Am Soc Nephrol*. 2002;13(7):1721–1732.
29. Rosenberger C, et al. Up-regulation of HIF in experimental acute renal failure: evidence for a protective transcriptional response to hypoxia. *Kidney Int*. 2005;67(2):531–542.
30. Kobayashi H, et al. Distinct subpopulations of FOXD1 stroma-derived cells regulate renal erythropoietin. *J Clin Invest*. 2016;126(5):1926–1938.
31. Traykova-Brauch M, et al. An efficient and versatile system for acute and chronic modulation of renal tubular function in transgenic mice. *Nat Med*. 2008;14(9):979–984.
32. Eremina V, et al. VEGF inhibition and renal thrombotic microangiopathy. *N Engl J Med*. 2008;358(11):1129–1136.
33. Kapitsinou PP, et al. Preischemic targeting of HIF prolyl hydroxylation inhibits fibrosis associated with acute kidney injury. *Am J Physiol Renal Physiol*. 2012;302(9):F1172–F1179.
34. Schley G, et al. Hypoxia-inducible transcription factors stabilization in the thick ascending limb protects against ischemic acute kidney injury. *J Am Soc Nephrol*. 2011;22(11):2004–2015.
35. Castrillon DH, Miao L, Kollipara R, Horner JW, DePinho RA. Suppression of ovarian follicle activation in mice by the transcription factor Foxo3a. *Science*. 2003;301(5630):215–218.
36. Andeen NK, Nguyen TQ, Steegh F, Hudkins KL, Najafian B, Alpers CE. The phenotypes of podocytes and parietal epithelial cells may overlap in diabetic nephropathy. *Kidney Int*. 2015;88(5):1099–1107.
37. Hong Q, et al. Increased podocyte Sirtuin-1 function attenuates diabetic kidney injury. *Kidney Int*. 2018;93(6):1330–1343.
38. Klotz LO, Sánchez-Ramos C, Prieto-Arroyo I, Urbánek P, Steinbrenner H, Monsalve M. Redox regulation of FoxO transcription factors. *Redox Biol*. 2015;6:51–72.
39. Nath KA, Croatt AJ, Hostetter TH. Oxygen consumption and oxidant stress in surviving nephrons. *Am J Physiol*. 1990;258(5 Pt 2):F1354–F1362.
40. Fine LG, Norman JT. Chronic hypoxia as a mechanism of progression of chronic kidney diseases: from hypothesis to novel therapeutics. *Kidney Int*. 2008;74(7):867–872.
41. Hirakawa Y, Tanaka T, Nangaku M. Renal Hypoxia in CKD; Pathophysiology and Detecting Methods. *Front Physiol*. 2017;8(99):eCollection 2017.
42. Kroemer G, Mariño G, Levine B. Autophagy and the integrated stress response. *Mol Cell*. 2010;40(2):280–293.
43. Morselli E, et al. The life span-prolonging effect of sirtuin-1 is mediated by autophagy. *Autophagy*. 2010;6(1):186–188.
44. Anderson MJ, Viars CS, Czekay S, Cavenee WK, Arden KC. Cloning and characterization of three human forkhead genes that comprise an FKHR-like gene subfamily. *Genomics*. 1998;47(2):187–199.
45. Biggs WH, Cavenee WK, Arden KC. Identification and characterization of members of the FKHR (FOX O) subclass of winged-helix transcription factors in the mouse. *Mamm Genome*. 2001;12(6):416–425.
46. Furuyama T, Nakazawa T, Nakano I, Mori N. Identification of the differential distribution patterns of mRNAs and consensus binding sequences for mouse DAF-16 homologues. *Biochem J*. 2000;349(Pt 2):629–634.
47. Jacobs FM, van der Heide LP, Wijchers PJ, Burbach JP, Hoekman MF, Smidt MP. FoxO6, a novel member of the FoxO class of transcription factors with distinct shuttling dynamics. *J Biol Chem*. 2003;278(38):35959–35967.
48. Greer EL, Brunet A. FOXO transcription factors at the interface between longevity and tumor suppression. *Oncogene*. 2005;24(50):7410–7425.
49. Huang H, Tindall DJ. Dynamic FoxO transcription factors. *J Cell Sci*. 2007;120(Pt 15):2479–2487.
50. Greer EL, Brunet A. FOXO transcription factors in ageing and cancer. *Acta Physiol (Oxf)*. 2008;192(1):19–28.
51. Hu MC, et al. IkappaB kinase promotes tumorigenesis through inhibition of forkhead FOXO3a. *Cell*. 2004;117(2):225–237.
52. Berra E, Benizri E, Ginouvès A, Volmat V, Roux D, Pouysségur J. HIF prolyl-hydroxylase 2 is the key oxygen sensor setting low steady-state levels of HIF-1alpha in normoxia. *EMBO J*. 2003;22(16):4082–4090.
53. Takeda K, Ho VC, Takeda H, Duan LJ, Nagy A, Fong GH. Placental but not heart defects are associated with elevated hypoxia-inducible factor alpha levels in mice lacking prolyl hydroxylase domain protein 2. *Mol Cell Biol*. 2006;26(22):8336–8346.
54. Lee S, et al. Neuronal apoptosis linked to EglN3 prolyl hydroxylase and familial pheochromocytoma genes: developmental culling and cancer. *Cancer Cell*. 2005;8(2):155–167.
55. Bruick RK, McKnight SL. A conserved family of prolyl-4-hydroxylases that modify HIF. *Science*. 2001;294(5545):1337–1340.
56. Epstein AC, et al. C. elegans EGL-9 and mammalian homologs define a family of dioxygenases that regulate HIF by prolyl hydroxylation. *Cell*. 2001;107(1):43–54.
57. Ivan M, et al. HIFalpha targeted for VHL-mediated destruction by proline hydroxylation: implications for O2 sensing. *Science*. 2001;292(5516):464–468.
58. Appelhoff RJ, et al. Differential function of the prolyl hydroxylases PHD1, PHD2, and PHD3 in the regulation of hypoxia-inducible factor. *J Biol Chem*. 2004;279(37):38458–38465.
59. Heckmann BL, Boada-Romero E, Cunha LD, Magne J, Green DR. LC3-associated phagocytosis and inflammation. *J Mol Biol*. 2017;429(23):3561–3576.
60. Martinez J, et al. Microtubule-associated protein 1 light chain 3 alpha (LC3)-associated phagocytosis is required for the efficient clearance of dead cells. *Proc Natl Acad Sci U S A*. 2011;108(42):17396–17401.
61. Martinez J, et al. Noncanonical autophagy inhibits the autoinflammatory, lupus-like response to dying cells. *Nature*. 2016;533(7601):115–119.
62. Linkermann A. Nonapoptotic cell death in acute kidney injury and transplantation. *Kidney Int*. 2016;89(1):46–57.
63. Skouta R, et al. Ferrostatins inhibit oxidative lipid damage and cell death in diverse disease models. *J Am Chem Soc*. 2014;136(12):4551–4556.
64. Yagoda N, et al. RAS-RAF-MEK-dependent oxidative cell death involving voltage-dependent anion channels. *Nature*. 2007;447(7146):864–868.
65. Panieri E, Santoro MM. ROS homeostasis and metabolism: a dangerous liason in cancer cells. *Cell Death Dis*. 2016;7(6):e2253.
66. Kousteni S. FoxO1, the transcriptional chief of staff of energy metabolism. *Bone*. 2012;50(2):437–443.
67. Zhao J, et al. FoxO3 coordinately activates protein degradation by the autophagic/lysosomal and proteasomal pathways in atrophying muscle cells. *Cell Metab*. 2007;6(6):472–483.
68. Semenza GL. Hypoxia-inducible factors in physiology and medicine. *Cell*. 2012;148(3):399–408.
69. Semenza GL. A compendium of proteins that interact with HIF-1α. *Exp Cell Res*. 2017;356(2):128–135.

70. Liu J, et al. Hypoxia, HIF, and Associated Signaling Networks in Chronic Kidney Disease. *Int J Mol Sci*. 2017;18(5):E0950.
71. Kapitsinou PP, et al. Hepatic HIF-2 regulates erythropoietic responses to hypoxia in renal anemia. *Blood*. 2010;116(16):3039–3048.
72. Higgins DF, et al. Hypoxia promotes fibrogenesis in vivo via HIF-1 stimulation of epithelial-to-mesenchymal transition. *J Clin Invest*. 2007;117(12):3810–3820.
73. Humphreys BD, et al. Fate tracing reveals the pericyte and not epithelial origin of myofibroblasts in kidney fibrosis. *Am J Pathol*. 2010;176(1):85–97.
74. Kramann R, DiRocco DP, Humphreys BD. Understanding the origin, activation and regulation of matrix-producing myofibroblasts for treatment of fibrotic disease. *J Pathol*. 2013;231(3):273–289.
75. Loeffler I, Wolf G. Epithelial-to-Mesenchymal Transition in Diabetic Nephropathy: Fact or Fiction? *Cells*. 2015;4(4):631–652.
76. Li L, Zepeda-Orozco D, Black R, Lin F. Autophagy is a component of epithelial cell fate in obstructive uropathy. *Am J Pathol*. 2010;176(4):1767–1778.
77. Mori K, et al. Endocytic delivery of lipocalin-siderophore-iron complex rescues the kidney from ischemia-reperfusion injury. *J Clin Invest*. 2005;115(3):610–621.
78. Nickolas TL, et al. Sensitivity and specificity of a single emergency department measurement of urinary neutrophil gelatinase-associated lipocalin for diagnosing acute kidney injury. *Ann Intern Med*. 2008;148(11):810–819.